UNIVERSIDADE FEDERAL DE SANTA CATARINA

CENTRO DE CIÊNCIAS FÍSICAS E MATEMÁTICAS

PROGRAMA DE PÓS-GRADUAÇÃO EM OCEANOGRAFIA

Micael Fernando Broggio

Avaliação das propriedades termohalinas do modelo climático global BESM-OA2.5 em escala do Atlântico Sul

FLORIANÓPOLIS

2019

Micael Fernando Broggio

Avaliação das propriedades termohalinas do modelo climático global BESM-OA2.5 em escala do Atlântico Sul

Dissertação submetida ao Programa de Pós-Graduação em Oceanografia da Universidade Federal de Santa Catarina para a obtenção do título de Mestre em Oceanografia.

Orientador: Prof. Dr. Carlos Alberto Eiras Garcia

Coorientador: Prof. Dr. Renato Ramos da Silva

Florianópolis

2019

Micael Fernando Broggio

Avaliação das propriedades termohalinas do modelo climático global BESM-OA2.5 em escala do Atlântico Sul

O presente trabalho em nível de mestrado foi avaliado e aprovado por banca examinadora composta pelos seguintes membros:

Profa. Regina Rodrigues Rodrigues, Dra.
Universidade Federal de Santa Catarina

Prof. Luciano Ponzi Pezzi, Dr.
Instituto Nacional de Pesquisas Espaciais

Certificamos que esta é a **versão original e final** do trabalho de conclusão que foi julgado adequado para obtenção do título de mestre em Oceanografia.

_____
Prof. Dr. Paulo Roberto Pagliosa Alves
Coordenador do Programa

_____
Prof. Dr. Carlos Alberto Eiras Garcia
Orientador

Florianópolis, 25 de setembro de 2019.

AGRADECIMENTOS

Primeiramente agradeço a Deus, pela oportunidade de viver uma nova experiência e pela força e perseverança em superá-la.

Aos meus pais e minha irmã pelo amparo; pelas orações; pela preocupação e por tudo mais que me foi ofertado.

Aos meus amigos de longa data, amigos de laboratório e amigos repentinos que fizeram parte dessa caminhada. Foi uma grande parceria.

A Camila Sayuri Santos Obata, pelo incentivo e auxílio com a língua inglesa. Suas dicas foram essenciais em meu crescimento na escrita.

Ao meu orientador Prof. Dr. Carlos Alberto Eiras Garcia, por ver e acreditar em meu potencial; pela confiança ao abrir as portas de seu laboratório, ao suporte dado a mim mesmo com todo atraso gerado pela troca de projeto e pela paciência em momentos de dificuldades na escrita em inglês.

Ao meu coorientador Prof. Dr. Renato Ramos da Silva, por me orientar durante o primeiro ano do mestrado; por permitir de bom grado a troca de orientação e de projeto depois desse ano; por aceitar ser meu coorientador; e por ser parte do meu alicerce quando precisei durante esta nova pesquisa.

Aos professores da Pós-Graduação em Oceanografia, pela paciência e disposição em transmitir seus conhecimentos.

A fundação CAPES, pelo financiamento e fomento do estudo.

Ao povo brasileiro, que por meio de seus impostos, tornaram toda a minha caminhada possível.

A todos que fizeram parte direta e indiretamente deste momento.

RESUMO

Modelos climáticos globais (GCMs) são uma das principais ferramentas para o planejamento de atividades de mitigação para as mudanças climáticas, portanto, é primordial conhecer sua confiabilidade. Este trabalho tem como objetivo avaliar as propriedades termohalinas das simulações históricas e cenários (RCPs 4.5 e 8.5) do modelo Brazilian Earth System Model (BESM) no oceano Atlântico Sul. Foram feitas comparações entre quatro GCMs (HADGEM2-ES, MIROC-ESM-CHEM, MIROC5 e BESM) utilizando programas de monitoramento (sensores MODIS e SAC-D, GO-SHIP e MOVAR) e a reanálise ORAS5-ECMWF como referência. As avaliações foram feitas a partir de análises dos padrões espaciais, aplicação de métricas estatísticas e tendências temporais. Os resultados mostraram padrões de erros espaciais comuns a todos os modelos. A maior divergência do modelo BESM é caracterizada com erros sistemáticos de temperatura e salinidade, possivelmente atribuídos a fluxos de calor calculados incorretamente. Em subsuperfície, o modelo BESM realizou as melhores representações para a Água Intermediária Antártica e a Água Profunda do Atlântico Norte, porém, teve dificuldades em simular a Água Central do Atlântico Sul. Próximo à costa brasileira, o diagrama T-S do modelo BESM representou razoavelmente bem todas as massas de água da região. O modelo também demonstra boas representações ao longo da costa brasileira e regiões tropicais. As taxas de temperaturas históricas do modelo mostram as representações mais próximas dos dados de referência, todavia, os dados de salinidade apresentam as maiores divergências. A análise de campos de temperatura e salinidade dos modelos BESM e SMA (média dos modelos HadGEM2-ES, MIROC-ESM-CHEM, and MIROC5) revelaram magnitudes próximas nos cenários RCPs 4.5 e 8.5, entretanto, os erros sistemáticos encontrados nos dados históricos estão presentes nos cenários e ficam evidentes nos dados médios do modelo BESM.

Palavras-chave: Mudanças climáticas. Modelos climáticos globais. Avaliação de modelos. IPCC.

ABSTRACT

Global climate models (GCMs) are one of the main tools for planning mitigation activities in the global climate changing environment, thus, it is primordial to comprehend their reliability. This work aims to evaluate the historical and scenarios (RCPs 4.5 and 8.5) simulations of the Brazilian Earth System Model (BESM) for the thermohaline component in the South Atlantic Ocean. Comparisons were made between four GCMs (HADGEM2-ES, MIROC-ESM-CHEM, MIROC5, and BESM) using ocean monitoring programs and ORAS5-ECMWF data like the reference data. The assessments were made from spatial pattern analysis, statistical metrics and temporal trends. The results have shown common spatial pattern errors in all models. The BESM model's major divergence is characterized by systematic errors in the temperature and salinity, possibly attributed to the miscalculated heat fluxes. In the subsurface, the BESM model had the best representation for the Antarctic Intermediate Water and North Atlantic Deep Water, but the model had difficulties in simulating the South Atlantic Central Water. Near the Brazilian Coast, the T-S diagram with BESM thermohaline properties represented reasonable well all water masses in the region. The B model has also shown a good spatial representation of T-S properties along the Brazilian coast and Tropical region. The BESM temperature historical rates show closer representation to the reference data but the salinity rate diverged. The temperature and salinity fields of BESM and SMA (mean between HadGEM2-ES, MIROC-ESM-CHEM, and MIROC5) models revealed close magnitudes in the RCP 4.5 and 8.5 scenarios. However, the systematic errors found in the historical data are present in both scenarios and they were more evident in the BESM mean data.

Keywords: Climate changes. Global climate model. Model evaluation. IPCC.

LISTA DE FIGURAS

LISTA DE TABELAS

LISTA DE ABREVIATURAS E SIGLAS

AAIW – Antarctic Intermediate Water;

ACC – Antarctic Circumpolar Current;

AG – Argentine Gyre

AMA – All Models Average;

AR – Agulhas Retroflection;

ARP – Amazon River Plume;

B – BESM-OA2.5 model;

BC – Brazilian Current;

BMCZ – Brazil-Malvinas Confluence Zone;

BUS – Benguela Upwelling System;

CRMSE – Centered Root Mean Square Error;

GCM – Global Climate Model;

GG – Gulf of Guinea;

M1 – HadGEM2-ES model;

M2 – MIROC-ESM-CHEM model;

M3 – MIROC5 model;

NADW – North Atlantic Deep Water;

NRE – Normalized Relative Error;

PZ – Polar Zone;

R – Coefficient Correlation;

RMSE – Root Mean Square Error;

SACW – South Atlantic Central Water;

SASG – South Atlantic Subtropical Gyre;

SAF – Subantarctic Front;

SAZ – Subantarctic Zone;

SMA – Selected Models Average;

StdD – Standard Derivations;

STF – Subtropical Front;

STZ – Subtropical Zone;

TRE – Typical Relative Error;

TW – Tropical Water;

SUMÁRIO

1 INTRODUÇÃO

Modelos climáticos são ferramentas primordiais na previsão de cenários climáticos futuros. Desta forma, eles são tratados como ferramentas relevantes para o planejamento de ações de adaptação à mudança do clima, sendo imprescindível conhecer sua confiabilidade. Para isso, torna-se crucial a avaliação de desempenho destes, tanto individualmente, quanto coletivamente. Diante das consideráveis evoluções dos mesmos, com a ampliação de variáveis e processos ponderados; as diferenças entre modelos e observações são cada vez mais quantificadas, sendo utilizadas ferramentas denominadas "métricas de desempenho" (FLATO *et al.*, 2013).

O processo de avaliação e validação de um modelo é direto e pode ser feito por comparação entre os dados de saída do modelo e dados reais observados, ou comparados com saídas similares de outro modelo já consagrado. Com isso, são estudados os erros e incertezas encontrados nestas comparações (FLATO *et al.*, 2013).

Os modelos climáticos apresentam certas peculiaridades quando comparados com os demais modelos. Ao contrário das previsões meteorológicas, estes são utilizados para fazer projeções de longo prazo não sendo sujeitos a uma avaliação uniforme ao longo do tempo. A avaliação do modelo climático é, de certa forma, mais difícil do que avaliar a habilidade de modelos de previsões do tempo, porque os modelos climáticos resolvem um problema de valor de fronteira em oposição ao problema de valor inicial colocado na previsão do tempo. Em outras palavras, em modelos climáticos, os valores colocados como condição inicial são perdidos devido as simulações serem de longo prazo (semanas, meses ou anos), sendo necessário condições de contorno Isso obscurece a associação entre o tempo no modelo e o tempo na natureza, de modo que as previsões do modelo não podem ser comparadas com as observações no dia-a-dia ou mês a mês. Além disso, os modelos climáticos são usados principalmente para fazer projeções em prazos muito longos (décadas até séculos), e essas projeções não podem ser avaliadas diretamente, ou seja, não é possível se vivenciar o dia, e comparar suas características climáticas com a projeção feita pelo modelo, como é feito nas previsões meteorológicas (PINCUS *et al.*, 2008).

O *Coupled Model Intercomparison Project, phase 5* (CMIP5) foi um conjunto de experimentos de modelagem climática utilizado pelo IPCC para o *Fifth Assessment*

Report (AR5). As simulações históricas dos modelos climáticos globais (GMCs) participantes do AR5 foram realizadas entre os anos de 1850 e 2005, com início no período da segunda revolução industrial. As previsões foram desenvolvidas a partir de *Representation Concentration Pathway scenarios* (RCPs), e foram simulados no período de 2006 a 2100 (TAYLOR; STOUFFER; MEEHL, 2012, CHOU *et al.*, 2014). Estes cenários consideram diferentes incidências de radiação, variações nos gases do efeito estufa e de aerossóis na atmosfera, além de ponderar cobertura e uso do solo. Para o CMIP5, foram utilizados 4 cenários RCPs (2.5, 4.5, 6.5 e 8.5). O RCP 2.5 é o cenário mais ameno e o RCP 8.5, o mais drástico (MOSS *et al.*, 2010).

Os modelos do CMIP5 são ferramentas robustas que continuam sendo exploradas. Em escala global, Landerer, Gleckler and Lee (2013) analisaram e compararam campos de nível da superfície marinha derivados de 33 CMIP5 GCMs com dados altimétricos de satélites. Sallée *et al.* (2013) avaliaram a camada de mistura do inverno de modelos CMIP5 no Oceano Austral para dias atuais e projeções futuras. Seus resultados mostram simulações que representam a camada mais rasa e deslocada para o Equador quando comparado com dados observados. Perez *et al.* (2014) mensurou as habilidades dos GCMs (CMIP3 e CMIP5) em reproduzir a variabilidade interanual e as medias climatológicas de pressão ao nível do mar na região Nordeste do Atlântico, e encontrou os modelos mais qualificados para representar a região. Fathrio *et al.* (2017) investigaram como os modelos CMIP5 simulam a salinidade superficial no Oceano Índico. Sobre a área estudada, três dos cinco setores analisados apresentaram vieses sazonais e anuais para o conjunto multimodal, sobrestimando a região da Bacia de Benguela e subestimando o Oceano Índico Oeste e Sudeste.

O modelo *Brazilian Earth System Model* (BESM) foi elaborado atendendo aos critérios estabelecidos pelo CMIP5 de forma a simular o complexo comportamento do sistema acoplado oceano-atmosfera numa escala decenal com variações na concentração de gases do efeito estufa na atmosfera (NOBRE *et al.*, 2013). Segundos os mesmos autores, as simulações com o modelo BESM ao longo do século 21 mostram resultados coerentes, com mudanças no balanço de radiação do topo da atmosfera e acúmulo de energia no sistema terrestre (aquecimento), aumento global da temperatura superficial do mar e redução do gelo marinho.

Embora o modelo BESM não tenha sido avaliado durante o AR5 (FLATO *et al.*, 2013) pois ainda estava em fase de implementação, artigos têm sido publicados sobre o BESM. Por exemplo, Farias *et al.* (2013) utilizaram os resultados do BESM, integrado com o modelo biogeoquímico TOPAZ, para modelar a diferença de pressão parcial do CO2 entre oceano e atmosfera na bacia do Atlântico Sul ao longo de 10 anos (1996-2016). Estes autores encontraram domínio de fluxos positivos (oceano-atmosfera) de CO_2 para a região tropical e fluxos negativos (atmosfera-oceano) para médias latitudes. Chou *et al.* (2014) avaliaram o modelo regional climático ETA usando os modelos climáticos globais HadGEM2-ES, BESM, e MIROC5, para o período de 1961 a 1990. Giarolla *et al.* (2015) investigaram a dinâmica do oceano Atlântico Sul Tropical do modelo BESM em comparação com modelos globais acoplados. Apesar de alguns vieses, o modelo BESM representa com razoável precisão a variação da temperatura da superfície no Equador e a inclinação da termoclina na mesma região. Casagrande et al (2016) testaram a habilidade do BESM em representar o gelo marinho no Ártico quando forçado pelas concentrações de CO2 na atmosfera, usando simulações decenais entre 1980 e 2012 e cenários futuros (2006-2100). Para os cenários, todos os modelos representaram diminuição na extensão do gelo marinho em resposta a um aumento na forçante radiativa.

Com este estudo, buscamos avaliar as propriedades termohalinas do GCM BESM-OA2.5 em escala do Atlântico Sul, utilizando métricas estatísticas para as análises (média, desvio padrão, coeficiente de correlação de Pearson [R], erro quadrático médio [RMSE], erro quadrático médio centrado na média [CRMSE], erro médio [BIAS]), além de estabelecer o erro relativo normalizado. Os processamentos básicos metodologicamente utilizados são descritos por Taylor (2001), Pincus *et al.* (2008) e Gleckler, Taylor and Doutriaux (2008). Além da análise estatística, o estudo também visa identificar padrões de erros espaciais que sejam atípicos aos demais modelos analisados, e ressaltar divergências apresentadas pelo modelo BESM, além de calcular as tendências temporais para cada GCMs.

As aplicações estatísticas foram realizadas nas comparações entre a reanálise ORAS5-ECMWF e dados históricos/cenários (1979 a 2017) de 3 GCMs (HadGEM2-ES, MIRO-ESM-CHEM, e MIROC5), além do modelo BESM. Outras análises foram realizadas entre GCMs na análise dos cenários RCPs; programas de

monitoramentos, como GO-SHIP, MOVAR; e sensores satelitais (MODIS e AQUARIUS). Tais bancos de dados são descritos a seguir.

1.1 MODELOS CLIMÁTICOS GLOBAIS UTILIZADOS NESTE TRABALHO

• BESM-OA2.5: BESM é um GCM acoplado, constituído do modelo de circulação atmosférica global do CPTEC/INPE acoplado ao modelo de circulação oceânica global GFDL (Geophysical Fluid Dynamics Laboratory) Modular Ocean Model version 4p1 (MOM4p1). As componentes da atmosfera e do oceano são descritas em detalhes por Nobre *et al.* (2013). A componente oceânica possui uma resolução horizontal uniforme de 1º ao longo da longitude. A grade latitudinal é variável; entre 10º S e 10º N, a resolução é de 1/4º e decresce uniformemente de 1º na latitude de 45º a 2º na latitude de 90º. Sua resolução vertical é de 50 níveis, com resolução de 10m nos 200m superiores da coluna de água, diminuindo de acordo com a profundidade. O módulo atmosférico tem resolução uniforme de 1,875° x 1,875°. O modelo é forçado por ventos, temperatura, umidade específica a 10m, pressão atmosférica, fluxos radiativos, cobertura e espessura de gelo e descarga de rios (NOBRE *et al.*, 2013).

• HadGEM2-ES: O modelo HadGEM2-ES é um modelo climático global acoplado. Este incorpora diferentes níveis de complexidades em suas diversas versões. A resolução atmosférica é de 1,875° x 1,275° na longitudinal e na latitudinal, e 37 níveis atmosféricos. O módulo oceânico tem 40 níveis na vertical, e varia de 1/3° nos trópicos para 1° em latitudes superiores à 30°. Este inclui, além das tradicionais componentes de sistemas AOGMCs (Atmosphere–Ocean General Circulation Models), componentes como aerossóis, dinâmica de vegetação, biogeoquímica oceânica e química atmosférica (COLLINS *et al.*, 2011; MARTIN *et al.*, 2011, FLATO *et al.* 2013; CHOU *et al.*, 2014).

• MIROC-ESM-CHEM: Desenvolvido por uma cooperação entre a universidade de Tokyo, NIES (National Institute for Environmental Studies), e JAMSTEC (Japan Agency for Marine-Earth Science and Technology); o MIROC também é um modelo acoplado, sendo ESM-CHEM, a versão mais robusta do mesmo. Este sistema de reprodução terrestre pondera componentes como atmosfera; oceano; superfície terrestre; gelo marinho; aerossóis; química atmosférica, carbono terrestre e

biogeoquímica marinha. No oceano, este possui 44 níveis e sua resolução latitudinal tem refinamento gradual, com menor resolução nos polos (1.7°) e maior resolução no equador (0.5°). A resolução longitudinal é constante (1.4°). Na atmosfera a resolução é de 2.8 x 2.8° (WATANABE *et al.*, 2011; FLATO *et al.* 2013).

  • MIROC5: O MIROC5 é um modelo similar ao MIROC-ESM-CHEM, porém, com menor número de componentes calculadas. Este não possui química atmosférica, carbono terrestre e biogeoquímica marinha. No oceano, o modelo possui projeção estereográfica polar com resolução zonal fixa (1,4°), 49 níveis e resolução meridional de 0.5° entre as latitudes de 0 a 8°, que cresce continuamente até o valor máximo de 1.4° (latitude de 65°), permanecendo nesta resolução até as máximas latitudes. Na atmosfera, sua resolução é de 1.4 x 1.4° (WATANABE *et al.*, 2010, FLATO *et al.* 2013).

1.2 PROGRAMAS DE MONITORAMENTO DO OCEANO

  • GO-SHIP: GO-SHIP é um programa estabelecido pelo IOCCP e CLIVAR para desenvolver uma estratégia de um programa sustentável de observações hidrográficas repetidas em escala global. Trata-se de um programa internacional em que cruzeiros de larga escala onde seções hidrográficas são conduzidas como parte do sistema de observação global dos oceanos e clima. O GO-SHIP inclui, portanto, medições que envolvem a oceanografia física, o ciclo do carbono, biogeoquímica marinha e os ecossistemas. Os dados hidrográficos do GO-SHIP possuem uma frequência aproximadamente decenal. Os dados coletados nas diferentes bacias oceânicas e regiões costeiras são de altíssima qualidade e os protocolos de medição foram elaborados para detectar mudanças em suas propriedades devido a mudanças climáticas globais (HOOD *et al.* 2010).

  • MOVAR: Junto ao programa GOOS-Brasil (The Global Ocean Observing System), o projeto MOVAR foi proposto em 2004, devido à pouca disponibilidade de dados referente à porção oceânica ao sul da Cadeia-Submarina de Vitória-Trindade. Os dados de temperatura são coletados na seção designada pela NOAA (National Oceanic and Atmospheric Administration) como AX97, sendo restritos aos primeiros 700 m de profundidade, perfilando a região entre a quebra da plataforma continental e a ilha de Trindade - ES. A aquisição é realizada com XBT (batitérmicos descartáveis)

e conta com uma resolução de aproximadamente 15 milhas náuticas entre estações (VAN CASPEL; MATA; CIRANO, 2010; GOOS-BR, 2018).

1.3 MISSÕES SATELITAIS

• MODIS AQUA/TERRA: O sensor Moderate Resolution Imaging Spectroradiometer (MODIS) é o equipamento mais robusto acoplado nas missões EOS-AM1 (satélite TERRA) e PM1 (satélite AQUA), tendo este, a capacidade de observar aproximadamente toda a superfície terrestre em dois dias, utilizando 36 bandas espectrais, com resolução espacial de 250, 500 ou 1000m dependendo da banda espectral (BARNES; PAGANO; SALOMONSON, 1998).

• SAC-D AQUARIUS: O objetivo principal desta missão foi prover dados superficiais mensais de salinidade para o globo, gerando subsídios para melhoramento de previsões climáticas sazonais e interanuais, além de auxiliar nas estimativas do orçamento hidrológico global e possibilitar a análise de salinidade em larga escala (LAGERLOEF *et al.*, 2008). O mesmo tem resolução espacial de 100 - 300km e cobre a superfície terrestre em 7 dias, fazendo este ciclo por aproximadamente 4 vezes em um mês (LAGERLOEF *et al.*, 2008).

2 OBJETIVOS

2.1 OBJETIVO GERAL

Avaliar as propriedades termohalinas das saídas históricas e de cenários (RCPs 4.5 e 8.5) do modelo climático global BESM em escala regional, perante a avaliação estatística e a representatividade espacial superficial e subsuperficial do Oceano Atlântico Sul, em especial para sua margem Oeste.

2.2 OBJETIVOS ESPECÍFICOS

• Averiguar a confiabilidade da reanálise ORAS5 – ECMWF para seu uso como dado referência para o estudo;

• Avaliar de forma estatística o desempenho do modelo BESM nos experimentos históricos/cenários sugeridos pelo IPCC (CMIP5);

• Investigar padrões atípicos de erros do modelo climático global BESM em comparação aos demais modelos analisados;

• Comparar as saídas dos cenários RCP 4.5 e 8.5 do modelo climático global BESM aos demais modelos analisados;

• Avaliar a capacidade de representação das massas d'água do modelo climático global BESM na margem ocidental do oceano Atlântico Sul;

Micael Fernando Broggio

Thermohaline properties evaluation of four global climate models, including BESM-OA2.5, in the South Atlantic Ocean

Esta seção é destinada à apresentação do artigo científico desenvolvido e submetido à revista: Journal of Geophysical Research: Oceans, como parte dos requisitos para a obtenção do Grau de Mestre em Oceanografia pela Universidade Federal de Santa Catarina.

Florianópolis

2019

1 INTRODUCTION

Global climate models (GCMs) are the main tools to project future climate scenarios. They are a relevant resource for planning actions of climate change adaptations, but it is indispensable to know their reliability. Therefore, individual and collective evaluation of GCM is crucial (FLATO *et al.*, 2013) to improve the understanding of the models' strengths and weaknesses. In the evaluation process, preterit model outputs have to be compared with observed data in which errors and uncertainties have to be quantified (FLATO *et al.*, 2013).

Instead of weather forecasts, climate models are used to produce long-term projections, therefore, the evaluation procedures are not uniform over time. In weather forecasts, short-term projections solve the initial value problem, unlike climate models that solve boundary value problems, which makes difficult to compare them to day by day or month by month observations. Additionally, the timescale of scenarios produced by climate models that range from decades to centuries cannot be compared directly to day-by-day prediction as in weather forecasts (PINCUS *et al.*, 2008).

The Coupled Model Intercomparison Project phase 5 (CMIP5) is a climate modeling experiment used by IPCC to the Fifth Assessment Report (AR5) (TAYLOR; STOUFFER; MEEHL, 2012). The AR5 GCMs simulations ranged from the modern industrial period (1850) until 2005. For the future scenarios, the Representation Concentration Pathway scenarios (RCPs) were used to simulate the period from 2006 to 2100 (CHOU *et al.*, 2014; TAYLOR; STOUFFER; MEEHL, 2012). These scenarios consider different future radiative forcing, greenhouses gases, aerosols availability, land use, and land cover. Four RCPs (2.5, 4.5, 6.5 and 8.5) are taken into account in which RCP 2.5 is the mildest scenario and RCP 8.5 is the most drastic scenario (MOSS *et al.*, 2010).

The CMIP5 models are robust tools and still explored nowadays. On a global scale, Landerer, Gleckler and Lee (2013) analyzed and compared the sea surface height fields derived from 33 CMIP5 GCMs with satellite altimetry data. Sallée *et al.* (2013) assessed the present-day and future projected changes in the Austral Ocean mixed layer of CMIP5 models. The simulations represent the shallower mixed layer and shifted equatorward compared to observations. Perez *et al.* (2014) measured the skill of GCMs (CMIP3 and CMIP5) to reproduce the interannual variability and mean

climatology of sea level pressure in the North-East Atlantic region and found the most qualified models to represent the region. Fathrio *et al.* (2017) investigated how the CMIP5 models simulate the surface salinity in the Indian Ocean. Three of the five sectors analyzed presented seasonal and annual biases for the multimodal ensemble, overestimating the Bay of Bengal region and underestimating the Western and Southeastern Indian Ocean.

The Brazilian Earth System Model (BESM) was elaborated following the CMIP5 criteria. The system is composed by ocean, atmosphere and sea ice coupled model with greenhouse gas concentration changes (NOBRE *et al.*, 2013). The model couples an atmospheric model (CPTEC/INPE Atmosphere Global Climate Model) with the Modular Ocean Model (MOM). According to Nobre *et al.* (2013), the BESM simulations throughout the 21st century have shown coherent results for the earth's top-of-atmosphere radiation balance changes, sea surface temperature increase, and marine ice reduction.

Embora o modelo BESM não tenha sido avaliado durante o AR5 pois ainda estava em fase de implementação, artigos têm sido publicados sobre o BESM. Por exemplo, Farias *et al.* (2013) utilizaram os resultados do BESM, integrado com o modelo biogeoquímico TOPAZ, para modelar a diferença de pressão parcial do CO2 entre oceano e atmosfera na bacia do Atlântico Sul ao longo de 10 anos (1996-2016). Estes autores encontraram domínio de fluxos positivos (oceano-atmosfera) de CO_2 para a região tropical e fluxos negativos (atmosfera-oceano) para médias latitudes. Chou *et al.* (2014) avaliaram o modelo regional climático ETA usando os modelos climáticos globais HadGEM2-ES, BESM, e MIROC5, para o período de 1961 a 1990. Giarolla *et al.* (2015) investigaram a dinâmica do oceano Atlântico Sul Tropical do modelo BESM em comparação com modelos globais acoplados. Apesar de alguns vieses, o modelo BESM representa com precisão a variação da temperatura da superfície no Equador e a inclinação da termoclina na mesma região. Casagrande et al (2016) testaram a habilidade do BESM em representar o gelo marinho no Ártico quando forçado pelas concentrações de CO2 na atmosfera, usando simulações decenais entre 1980 e 2012 e cenários futuros (2006-2100). Para os cenários, todos os modelos representaram diminuição na extensão do gelo marinho em resposta a um aumento na forçante radiativa.

The BESM model has not been used during AR5 because it was in its implementation phase, but several studies have been conducted in recent years. Farias *et al.* (2013) have integrated the BESM model with the Tracers of Phytoplankton with Allometric Zooplankton (TOPAZ) model to measure the variability of air-sea CO_2 fluxes in the South Atlantic between 1996 and 2016. These authors found positive CO_2 fluxes (sea-to-air) dominating over the Tropical region and negative fluxes (air-to-sea) in mid-latitudes regions. Chou *et al.* (2014) evaluated the ETA regional climate model using the BESM-OA2.3, HadGEM2-ES, and MIROC global models as a large-scale forcing. Giarolla *et al.* (2015) explored the Tropical South Atlantic Ocean dynamic given by the BESM model in comparison with coupled global models. Despite some systematic errors, the BESM model represented accurately the Equatorial surface temperature variation and the slope of the equatorial thermocline (east-west). Casagrande *et al.* (2016) evaluated the ability of the BESM model to reproduce Arctic ice-sea variability between 1980 and 2012, and in futures scenarios between 2006 and 2100. For the scenarios, all models simulated the decrease in the ice sea extent in response to an increase in radiative forcing.

In this work, we evaluated the temperature and salinity fields in the South Atlantic Ocean (SAO) using the BESM-OA2.5 model and three other GCMs. The statistical analysis employed here involves a comparison between the ORAS5-ECMWF reanalyzes (considered as reference data) and GCM historical/scenarios records of four global climate models (HadGEM2-ES [M1], MIRO-ESM-CHEM [M2], MIROC5 [M3]), and BESM [B]). We performed additional analyses between GCM (with different RCPs) outputs and data from ocean monitoring programs (GO-SHIP and MOVAR), and satellite data (MODIS and SACD). Besides the statistical evaluation, this study seeks to identify error patterns atypical to other models analyzed with an emphasis on differences presented by the BESM model.

2   DATA SETS AND METHODS

2.1   STUDY AREA

The study area covers the tropical and South Atlantic Ocean (SAO) and is limited between 60°S to 25°N and 70°W to 20°E, with an emphasis on the western

region (Figure 1). In this region, the meridional heat transfer from south to north occurs in the SAO with a great contribution to the global thermohaline circulation by the Atlantic Meridional Overturning Circulation (AMOC) (GARZOLI; MATANO, 2011; PEZZI; SOUZA; QUADRO, 2016). The most prominent feature in SAO is the South Atlantic Subtropical Gyre (SASG), where anticyclonic surface currents are wind-driven and resembles the atmospheric circulation in the South Atlantic, e.g. South Atlantic Subtropical High (MARCELLO; WAINER; RODRIGUES, 2018; PEZZI; SOUZA, 2009; PEZZI; SOUZA; QUADRO, 2016; TALLEY *et al.*, 2011; STRAMMA; ENGLAND, 1999).

Figure 1. The study area showing the lines of A10 (red line), A16 (red) and MOVAR (blue) of the ocean monitoring programs GO-SHIP (A10 and A16) and MOVAR in the South Atlantic.
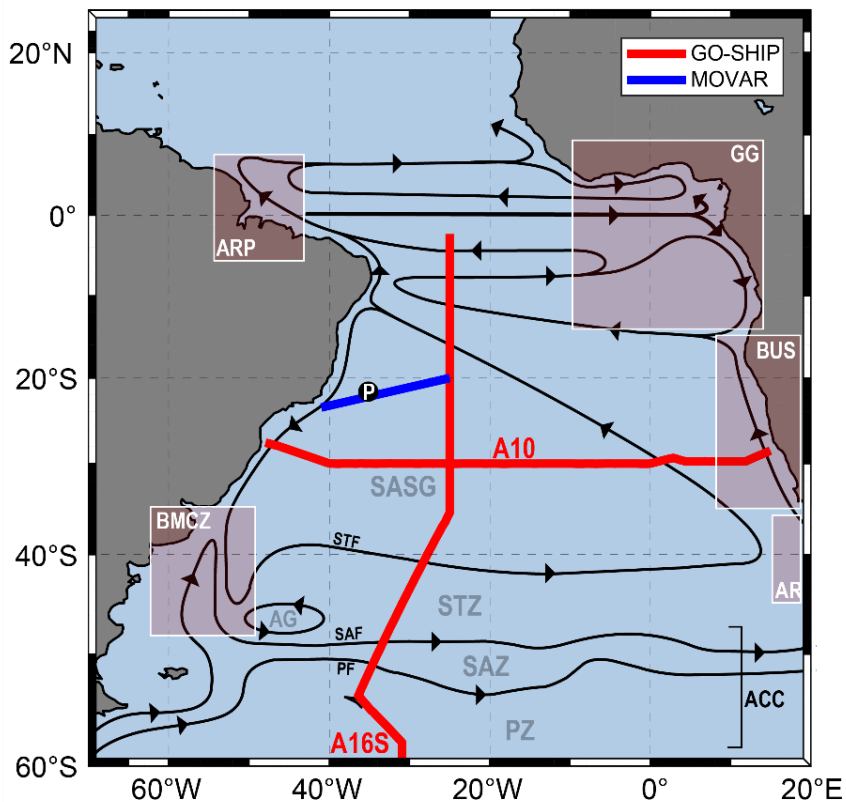
Adapted from Peterson and Stramma (1991).

A westward flow in the northern side of SAO characterizes the surface circulation, called the South Equatorial Current. In the western boundary, the Brazilian Current (BC) flows southward along the South America coast. On the southwestern side, the South Atlantic Current flows eastward. On the eastern side, the Benguela

Current flows northward forming the Benguela upwelling system (BUS) (PETERSON; STRAMMA, 1991; TALLEY *et al.*, 2011). Further south of SASG, the Antarctic Circumpolar Current (ACC) flows eastward, with the Subantarctic Front (SAF) as its northern frontier. These Pacific water masses enter the SAO through the Drake Passage and one branch flows northward as the Malvinas/Falkland Current. The interaction between the Malvinas Current and the BC occurs between 36 and 38°S, the so-called Brazil-Malvinas Confluence Zone (BMCZ) (TALLEY *et al.*, 2011). The Agulhas Retroflection (AR) is another mechanism of water mass entry in SAO, where warm waters enter from the Indian Ocean and help to promote a distinct meridional heat transfer (GORDON, 1986). The SAO also receives an enormous amount of freshwater from the discharge of the Amazon River, beyond of La Plata River, the second largest river in South America, and the African rivers of Congo, Niger, Ogooué and Sanaga in the Gulf of Guinea (GG) (BERGER *et al.*, 2014; PIOLA *et al.*, 2005; TZOETZI *et al.*, 2013). In general, the water masses in the 0-3000m depth found in BC region are: Tropical Water (TW) (θ>20°C and SO>36), South Atlantic Central Water (SACW) (6°<θ<20°C and 34.6<SO<36), Antarctic Intermediate Water (AAIW) (3°<θ<6°C; 34.2<SO<34.6), and North Atlantic Deep Water (NADW) (3°< θ<4°C and 34.6<S<35) (MÖLLER, 2008; PEREIRA *et al.*, 2014, PIOLA; MATANO, 2017; ROSSI-WONGTSCHOWSKI; MADUREIRA, 2006; SILVEIRA *et al.*, 2000).

Figure 1 also shows the transects of repeated oceanographic cruise whose ocean data will be used in the evaluation process. The A10 GO-SHIP is a zonal cruise, which crosses the SAO and it extends between ~50°W and ~15°E with a mean latitude of 30°S, sampling regions in the SASG center and BUS. The A16S GO-SHIP is a near meridional cruise that samples from the Equatorial Zone, crossing the SASG center toward the Antarctic Circumpolar Current (~0 to 60°S).

The MOVAR transect occurs between Rio de Janeiro city up to Vitoria-Trindade Chain and until now, 72 transects took place in the area. The Vitoria-Trindade Chain has east-west orientation, with two outcrops, the Trindade and Martin Vaz islands, that work as a BC flux barrier (GOES *et al.*, 2017).

2.2   DATA SETS

We used multiple data sources in this study. Table 1 shows the data sets, the abbreviations used in the study and the period of data in the evaluation procedure. The variables SST, θ, SSS and SO stand for surface temperature (°C), potential temperature (°C), surface salinity, and subsurface salinity, respectively.

Table 1. Data sets used in this work.

Origin	Data source	Symbol	Variable	Period of Time Series
Reanalysis/ Observed	ECMWF-ORAS5	ORAS5	SST; θ; SSS; SO	1979 – 2017
Models	BESM-OA2.5	B	SST; θ; SSS; SO	1979 – 2098
	HadGEM2-ES	M1	SST; θ; SSS; SO	1979 – 2098
	MIROC-ESM-CHEM	M2	SST; θ; SSS; SO	1979 – 2098
	MIROC5	M3	SST; θ; SSS; SO	1979 – 2098
	All models average (B, M1, M2, M3)	AMA	SST; θ; SSS; SO	1979 – 2098
	Selected models average (M1, M2, M3)	SMA	SST; θ; SSS; SO	1979 – 2098
Satellite	MODIS Aqua/Terra	MODIS	SST	2003 – 2017
	SAC-D Aquarius	SACD	SSS	2012 – 2014
Ocean Monitoring Programs	MOVAR	MOVAR	θ; SO	2005 – 2017
	GO-SHIP	GO-SHIP	θ; SO	A10 – 2011 A16S – 2013

2.2.1   The Reference Data

The Ocean Reanalysis System 5 (ORAS5) is the base of the main reference dataset used in this work. ORAS5 has been developed by the European Centre for Medium-Range Weather Forecasts (ECMWF) and the dataset fully description can be found in Zuo *et al.* (2019). The ORAS5 has a horizontal resolution of 0.25° latitude/longitude and 75 vertical levels, and here we used the monthly potential temperature and salinity from 1979 to 2017. In this work, a brief comparison was made between ORAS5 data and all the monitoring programs (GO-SHIP, MOVAR, MODIS Aqua/Terra and SACD Aquarius) to verify its consistency.

The GO-SHIP was created by the International Ocean Carbon Coordination Program (IOCCP) and Climate and Ocean: Variability, Predictability, and Change (CLIVAR) as a sustainable program of hydrographical observations on a global scale.

This program comprises large-scale cruises by hydrographical sections that constitute a global observing ocean and climate system. The GO-SHIP brings together data on physical hydrography, carbon cycle, marine biogeochemistry, and ecosystems. The measurements are made at an approximately decennial frequency and their protocols require a high-quality data sets from ocean and coastal regions (HOOD *et al.*, 2010).

The MOVAR monitoring program is part of the Global Ocean Observing System - Brazil (GOOS-Brazil) with measurements of potential temperature and inferred salinity from surface to 700m depth. XBT vertical profiles are obtained in a horizontal resolution of 15 miles, between Rio de Janeiro and Trindade Island (VAN CASPEL; MATA; CIRANO, 2010; GOES *et al.*, 2017). The MOVAR data spans from 2004 to 2018.

The Moderate Resolution Imaging Spectroradiometer (MODIS) is a sensor placed in EOS-AM1 and PM1 missions (AQUA and TERRA satellites). These sensors observe the earth's surface in two days, using 36 spectral bands, at a horizontal resolution of 250, 500 and 1000m, depending on the waveband (BARNES; PAGANO; SALOMONSON, 1998). In this work, we used the monthly 9 km resolution sea surface temperature from 2003 to 2017 provided by both satellites.

The SACD Aquarius was a mission to provide global surface salinity data, to generate subsidies to climate forecast, and to help to estimate global hydrological budget. The sensor has a spatial resolution of 100 to 300km and, it covers the earth's surface in 7 days, therefore, 4 turns per month (LAGERLOEF *et al.*, 2008). We used the monthly 1-degree resolution sea surface salinity from 2012 to 2014.

2.2.2 The GCMs Data

In this work, we used monthly-mean models output data to evaluate the Brazilian Earth System Model (BESM-OA2.5) and three GCMs provided by the CMIP5 experiment. The three additional GCMs models used are: Hadley Center Global Environment Model version 2 (HADGEM2-ES), Model for Interdisciplinary Research on Climate (MIROC5), and MIROC-ESM-CHEM. Table 2 provides information about each model used here. Further details on CMIP5 models can be obtained on the CMIP5 website (http://cmip-pcmdi.llnl.gov/cmip5/index.html).

28

Table 2. List of climate models used in historical analyzes and comparison scenarios.

Model Name	Institute	Resolution	Ensemble	Reference
BESM-OA2.5	National Institute for Space Research, Brazil	Ocean Latitude: 0° : 10° = 0.25° 10° : 45° = 0.25° : 1° 45° : 90° = 1° : 2° Longitude: 1° Atmosphere 1.875 x 1.875°	r1i1p1	NOBRE *et al.* (2013)
HadGEM2-ES	Met Office Hadley Center, UK	Ocean Latitude: 0° : 30° = 0.33° - 1° 30° : 90° = 1° Longitude: 1° Atmosphere 1.875 x 1.25°	r1i1p1	MARTIN *et al.* (2011) Collins *et al.* (2011)
MIROC-ESM-CHEM	Japan Agency for Marine-Earth Science and Technology; Atmosphere and Ocean Research Institute; The University of Tokyo; National Institute for Environmental Studies, Japan	Ocean Latitude: 0° : 90° = 0.5° - 1.7° Longitude: 1.4° Atmosphere 2.8 x 2.8°	r1i1p1	WATANABE *et al.* (2011)
MIROC5	Japan Agency for Marine-Earth Science and Technology; Atmosphere and Ocean Research Institute; The University of Tokyo; National Institute for Environmental Studies, Japan	Ocean polar stereographic projection Meridional: 0° : 8° = 1/2° 8° : 65° = 1/2° - 1.4° 65° : 90° = 1.4° Zonal: 1.4° Atmosphere 1.4 x 1.4°	r1i1p1	WATANABE *et al.* (2010)

2.3 PERFORMANCE EVALUATION OF THE GCMS

To evaluate the models' performance, we used the statistics described by Taylor (2001) and Pincus *et al.* (2008). We estimated the correlation coefficient (R), root mean square error (RMSE), centered root mean square error (CRMSE), and mean error (BIAS) between simulated and reference patterns as:

$$R = \frac{\frac{1}{N}\sum_{n=1}^{N}(m_n - \bar{m})(o_n - \bar{o})}{\sigma_m \sigma_o} \tag{1}$$

$$RMSE = \sqrt{\frac{\sum_{n=1}^{N}(m_n - o_n)^2}{N}} \tag{2}$$

$$CRMSE = \sqrt{\frac{\sum_{n=1}^{N}[(m_n - \bar{m}) - (o_n - \bar{o})]^2}{N}} \tag{3}$$

$$BIAS = \bar{m} - \bar{o} \tag{4}$$

where m_n and o_n are simulated and reference fields, respectively, $\bar{m}$ and $\bar{o}$ are mean of the simulated and reference fields means, σ_m and σ_o are standard derivation of the simulated and reference fields, n is the index summation and N is the final index (size of the time series).

The normalized relative error (NRE) was also calculated (Gleckler, Taylor and Doutriaux, 2008) as proposed by Pincus *et al.* (2008) is given by:

$$NRE = \frac{E_{mmo} - \bar{E}_{mo}}{\bar{E}_{mo}} \tag{5}$$

where $\bar{E}_{mo}$ is the typical model error (TME) of the median of N GCMs errors, and E_{mmo} is the particular model error in relation to the reference data set. The TME is the median of the all models' error that have been used in the analysis. These authors converted the statistics metrics to values with uniform variations. The statistical metrics errors are defined as 1-R, RMSE, CRMSE, |BIAS|, and |1-StdDev|.

Lastly, we calculated the 12 months moving average to find the linear trends. The monthly rates of each model were calculated using the difference between the last and the first data from linear regressions. We estimate de annual rates from the monthly rates.

3 RESULTS AND DISCUSSION

3.1 TEMPERATURE AND SALINITY SURFACE CLIMATOLOGY

Figure 2 exhibits the BIAS between the simulated and reference SST (°C) and SSS monthly climatology. Figures 2c and 2k show a comparison between MODIS/SACD and ORAS5, whereas comparison between GCMs and ORAS5 can be seen in Figure 2 [d-h and l-p]). The continuous contour lines drawn in Figures 2 [d-h and l-k] represent the 18 °C and 35 of the ORAS5, respectively while the dashed lines represent the same values of the evaluated GCMs. The 18 °C line contour represents approximately the position of the Subtropical front (STF).

The differences found between the mean climatology of SST-MODIS and SST-ORAS5 (Figure 2c) and of SSS-SACD and SSS-ORAS5 (Figure 2k) were considered low during the available periods for each sensor (MODIS/2003-2017 and SACD/2012-2014). Values close to 0 can be seen in the most part of the BIAS maps. From now on, we will take ORAS5 as reference data to evaluate the GCMs climatology.

In all GCM outputs, including the selected models average (SMA - mean between HadGEM2-ES [M1], MIROC-ESM-CHEM [M2], and MIROC5 [M3]), similar patterns with either positive or negative biases can be observed. These are common errors between all GCMs, including in the BESM (B) model climatology. Positive SST errors are visible at latitudes higher than 45° S in all GCMs (Figure 2d to 2h), with minor and major errors in M2 (+3°C) (Figure 2g) and B (+6°C) (Figure 2e) models, respectively. Positive SST biases are also found on the BUS and BMCZ. In the first, the outstanding SST BIAS was found in the B model, with errors of the order of +6ºC. In the BMCZ region, all GCMs showed similar bias magnitudes (+9ºC), which implies that the GCMs are not able to detect precisely the encounter of both Brazil and Malvinas Currents. Negative SST biases are notorious in Argentine Gyre (AG) in the Argentine basin and less intense in the Agulhas Retroflection. We observed more intense biases in the M2 model (Figure 2g) with values of -6 and -4°C in the Argentine Gyre and Agulhas Reflection regions, respectively. Figure 2l to 2p shows the SSS BIAS patterns. Errors are visible in all models, either negative or positive depending on the GCM, but overall SSS biases are negative in the SAO. The SSS is better represented than SST in the BUS area for all GCMs, however, errors in regions close to in runoff

rivers are also easily noticed. Oceanic regions close to large river discharges, such as the Gulf of Guinea region and the Amazon river plume (ARP) are not captured well by any of the GCMs. In the Amazon river plume region, SSS BIAS are greater than 3 for all GCMs. The BESM model (Figure 2m) presents a relatively high negative SSS BIAS around 35° S in the South Atlantic Current region.

A generalized warming occurs in the SST field for B model (Figure 2e) in practically all the studied area, except in the Equatorial zone, more specifically in the north of SASG and along the Brazilian coast. No negative errors are found in SST variable for the B model, but it exhibits slight positive or neutral bias in places where the other GCMs have shown negative biases (e.g., Argentine Gyre and Agulhas Retroflection). The overall systematic errors of all GCMs are better represented in Table 3, which shows the comparison of the SST (°C) and SSS variation rates for all simulated data sets between 1979 and 2017.

The B model simulations presented an accentuated climate sensitivity, which caused disturbance of approximately +1.5°C in their averages (Table 3). The climate sensitivity is derived from radiative forcing, and both factors are responsible for the climate response of the model. The radiative forcing, that refers to the disturb in question, and the climate sensitivity, is defined as the response of climate per variation unit of radiative forcing and is presented as the reference of the global mean temperature (BADER *et al.*, 2008). Since the SST is tightly restricted by the ocean and atmosphere interaction, some processes can interfere in the incident radiation, misrepresenting the SST response. An example is the parametrization of clouds (e.g. stratus and stratocumulus) that reflects the sunlight incidence, mostly in tropics and subtropics, or commonly associated with presence of oceanic cold water, such as upwelling zones (e.g. BUS region) (FLATO *et al.*, 2013; RANDALL *et al.*, 2007, ZHENG *et al.*, 2011). This assumption can be a possible answer for the systematic SST error, but there is a need to evaluate other parameters, such as clouds, heat flux, short and long-wave radiation and so on. Another hypothesis resides in physics deficiencies, as suggested by Nobre *et al.* (2013).

Figure 2. BIAS between the simulated and reference (ORAS5) SST (°C) (a-h) and SSS (i-p) monthly climatology in the South Atlantic Ocean. The values of 18 °C and 35 of salinity are represent in black line contours. The continuous and dashed lines represent the reference and simulated data, respectively. a) MODIS monthly climatology (2003-2017). b) ORAS5 monthly climatology (1979-2017). c) BIAS between MODIS sensor and ORAS5 using the 2003-2017 climatology. d to h) SST BIAS between GCMs and ORAS5 (1979-2017). The same description is applied to the SSS data in Figures i to p. Where is seen MODIS (2003-2017), read SACD (2012-2014). All data sets were interpolated to the same grid resolution (0.5° x 0.5°).
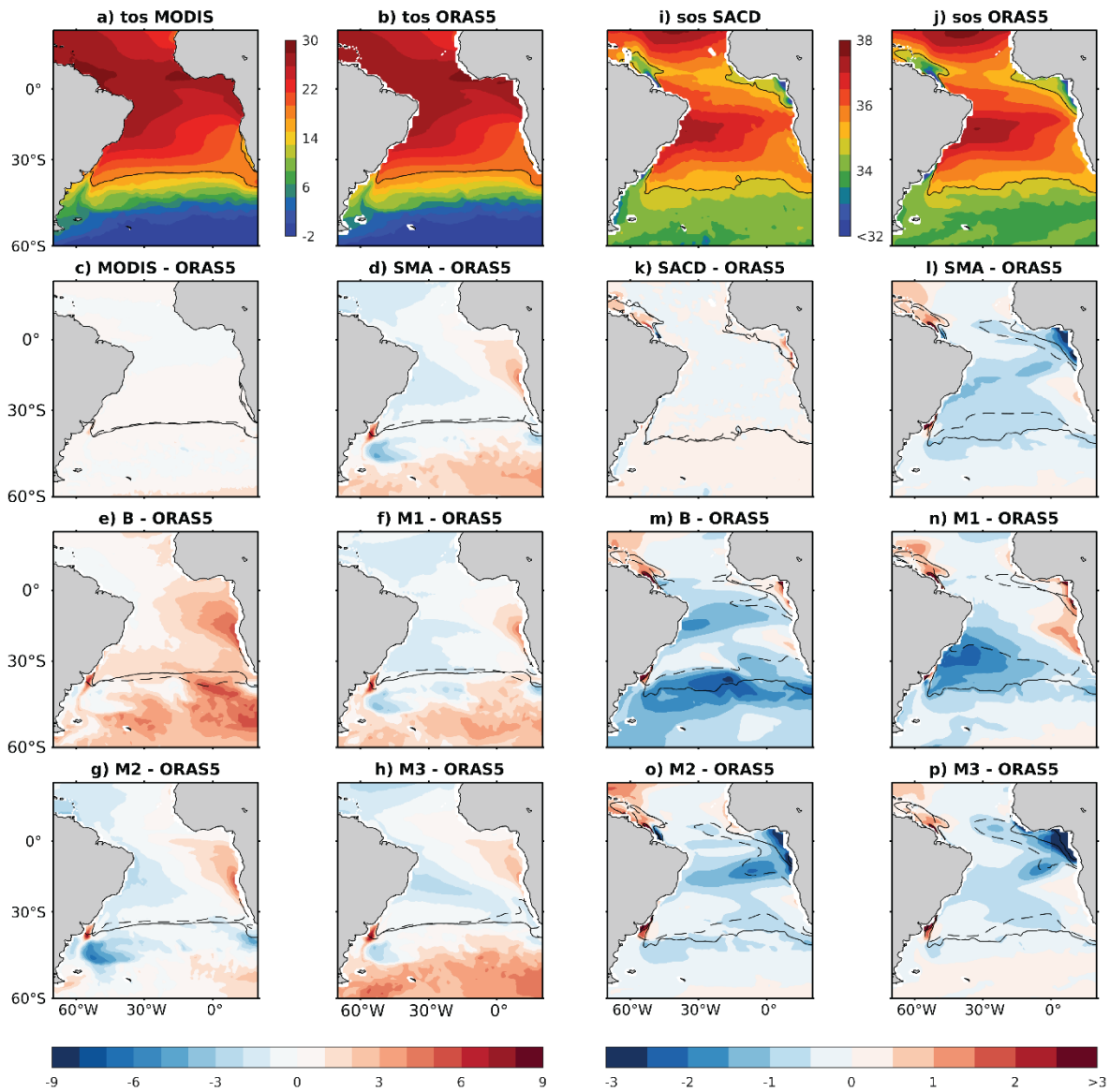
The salinity is more difficult to analyze because it is related to complex processes, such as the difference between evaporation and precipitation, ice formation and melting, river runoff, and vertical advection. These processes cause a great impact in the salinity variations; allowing errors to occur without control (BERGER *et al.*, 2014; FLATO *et al.*, 2013; SCHMITT, 1995; YU, 2011). Differently of SST biases of the B model, the differences in SSS patterns (Figure 2m) are visible in some specific regions.

We found some errors in the other GCMs too, with the same intensity, and location, like Amazon river plume, Gulf of Guinea, and BMCZ; however, two discrepant biases outstands. We observe the first and, less intense in near the Equatorial zone (~10°S) and, extend along the northeastern Brazilian coastal zone. The second and major is located in the Subtropical Zone (STZ) and the Subantarctic Zone (SAZ) (~40°S to 50°S), which probably cause overall low mean data due to its size. In both cases, the evaporation and precipitation processes have great influence on SST patterns, but with inverse behaviors. The evaporation outweighs the precipitation in near the Equatorial zone whereas the precipitation outweighs evaporation in the Subtropical front and high latitudes (MEEHL *et al.*, 2007; SCHMITT, 1995; DURACK; WIJFFELS; MATEAR, 2012). Thus, BIAS can be produced by major (minor) precipitation (evaporation) depending on the region. In the southern region, error may occur due to the decrease in the surface salinity, which tends to move the STZ and the SAZ to lower latitudes. Another possible explanation is the process of ice formation/melting; that can amplify the negative BIAS, even with the small errors shown in the Polar Zone (PZ).

Figure 3 and Table 3 show the comparison of the SST (°C) and SSS variation rates for all simulated data sets between 1979 and 2017, where the calculations were applied for the whole domain of the SAO. The Mann Kendall test was applied for the 0.95 significant level. The black box shows the data with insufficient evidence to reject the null hypothesis.

The annual rates of 0.008 °C/year and -0.0009 salt/year for SST and SSS, respectively, were found in the ORAS5 dataset (Table 3). The B model presented the SST annual rate of 0.012°C/year, the closest to the reference data among all models. However, the SSS annual rate (0.0019/year) was the worst among all models. The GCM M2 presented the best SSS annual rate among the GCMs.

It is possible to observe that systematic errors occur in all models (Figure 3). For the B model, these systematic errors are most accentuated in both variables, causing disturbances of about 1.6°C and -0.6 for SST and SSS (Table 3) in comparison with the ORAS5 data, respectively. This error is possibly caused due to the positive BIAS above 45° S and in the BUS regions, and the low estimated salinity in the STZ and SAZ.

Figure 3. Mean monthly SST (°C) and SSS from 1979 to 2017. The straight lines show the linear trends obtained for ORAS5, AMA, SMA, B, M1, M2, and M3 along the 38 years.
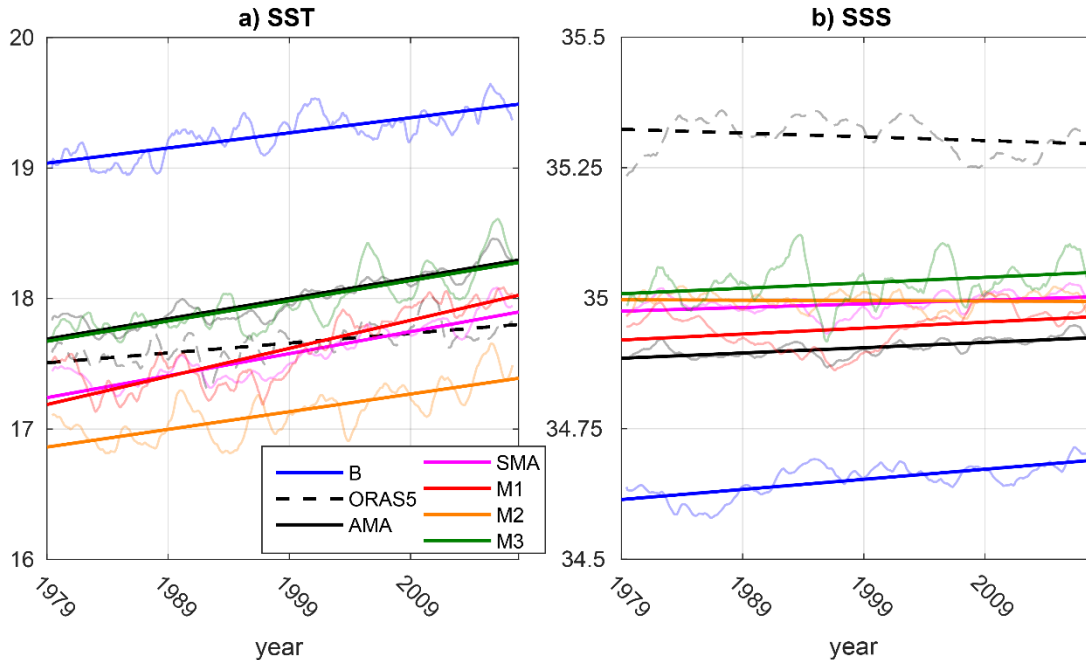
Table 3. Rate of variation of both mean annual SST (°C) and SSS (salt) and percentage of variation of SST and SSS over the 38 years (1979-2017) period. The color gradient represents the lowest (dark blue) to the highest (dark red) rate or value in comparison with reference data (ORAS5). PP = Physical Parameter.

PP	Rate	ORAS5	AMA	SMA	B	M1	M2	M3
SST	38yrs rate(°C/38years)	0.286	0.589	0.639	0.440	0.816	0.514	0.588
	Annual rate(°C/year)	0.008	0.016	0.017	0.012	0.021	0.014	0.015
	Mean (°C)	17.654	17.992	17.569	19.263	17.606	17.125	17.974
	Mann Kendall p-value	0	0	0	0	0	0	0
SSS	38yrs rate	-0.036	0.038	0.026	0.074	0.042		0.039
	Annual rate	-0.0009	0.0010	0.0007	0.0019	0.0011		0.0010
	Mean	35.311	34.905	34.989	34.651	34.941	34.997	35.030
	Mann Kendall p-value	0	0	0	0	0	0.629	0

Figure 4 exhibits the Hovmoller diagrams of monthly mean zonal biases of SST (°C) (Figures 4b to 4f) and SSS (Figures 4h to 4l) for the SAO between 1979 and 2017. The M2 model presented the best SST annual pattern (Figure 4e). M1, M3, and SMA models gave positive SST biases in the STZ and SAZ during all year (Figures 4b, 4d and 4e) while the B model presented the largest error in the region (Figure 4c). The BESM model BIAS (Figure 4c) presented certain seasonality, with a slight negative BIAS between July and November. Between the months of December and June, we

see an overheating in the summer season, with a maximum value (9°C) in February, with a temporal delay to the season. This overheating is possibly due to the systematic error previously detected and may be associated with errors in the radiation incidence in the region and convective clouds representation that generally occurs during the summertime. In the same model, we also identified positive BIAS (3 to 4°C) in latitudes between 0 and 30°S, possibly representing the BUS region. The Benguela upwelling presents seasonal variation, with north upwelling intensification in July and September, displacing to the southward at other times (HUTCHINGS *et al.*, 2009).

Figure 4. Hovmoller diagram of the monthly mean (1979-2017) zonal BIAS of SST (°C) (a-f) and SSS (g-l) in the South Atlantic Ocean between ORAS5 reanalysis and GCMs. a and g) Reference (ORAS5) SST and SSS monthly mean data; b-f and h-l) BIAS between ORAS5 and GCMs.
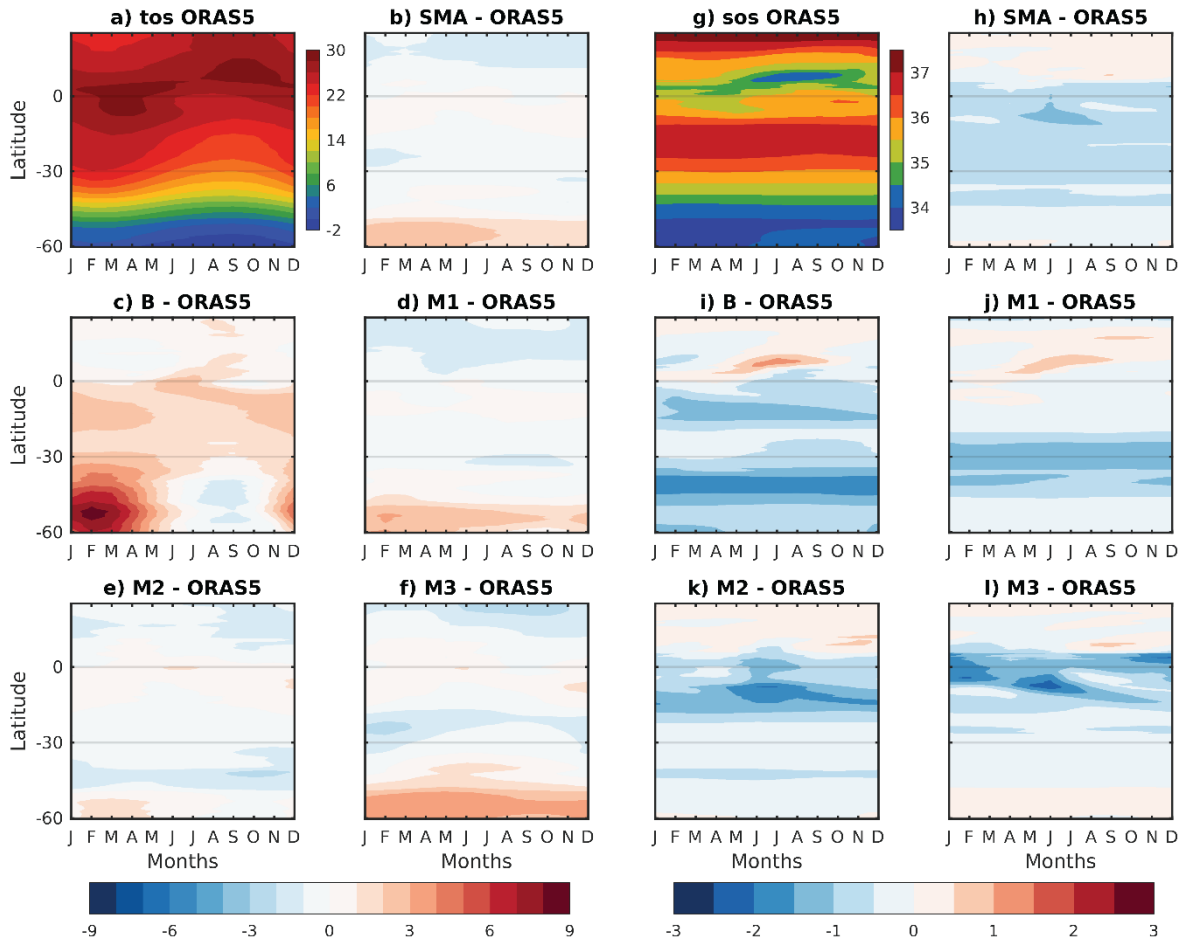
The SSS annual variation in ORAS5 data occurs in low latitudes near to the Equatorial zone with small amplitudes. Those low salinities are found between July and November near 10°N and between January and June at the equator with minor

intensity (Figure 4g). This polarization has also been reported by Tzortzi *et al.* (2013), and it is due to the increase in precipitation and peaks in river runoffs (Amazonas and Orinoco) especially at latitude ~10°N. The southern hemisphere (latitude 0°) receives freshwater increment from the rivers that flow to the Gulf of Guinea, but, these do not control the seasonal regime that is modulated by the vertical advection coming from BUS (BERGER *et al.*, 2014; YU, 2011). In the simulated periods, none of the models have demonstrated this variation. In the first case, the B and M1 models (Figures 4i and 4j) have failed with positive salinity biases between 0.5 to 1.5. In the second case, negative biases in M2 and M3 models were noticed (Figures 4k and 4l), because possibly they represented major runoff in the Gulf of Guinea and did not represent the northern intensification during the period in BUS. Especially for the B model (Figure 4i), the negative BIAS patterns in near to the Brazilian coast (~10°S) and in the STZ and SAZ were persistent during the year.

3.2   TEMPERATURE AND SALINITY SUBSURFACE CLIMATOLOGY

Figures 5 and 6 show the BIAS of the θ (°C) (Figures c to h) and SO (Figures k to p) properties for the A10 and A16S transects. The A10 profile is a zonal profile at latitude ~35°S, and the A16S profile is a meridional profile at longitudes between 25-35°W. Figures 5c/6c and 5k/6k show a comparison between GO-SHIP data and ORAS5 reference. The remaining figures show the evaluated BIAS between GCMs and ORAS5. Three contour lines are shown in these figures to emphasize the water mass interfaces based on Silveira *et al.* (2000) and Pereira *et al.* (2014).

In both Figures 5 and 6, we observe common errors in the layers near to the surface (above ~700m) in all GCMs, but with different intensities among them. Patterns of positive errors in θ are found in deep waters. The errors of the B model resemble the other models in simulating both physical properties; however, we observed small differences in the spatial patterns.

Figure 5. The BIAS between the simulated and reference (ORAS5) θ (Cº) (a-h) and so (l-p) monthly climatology in the South Atlantic Ocean at 30º S (GO-SHIP A10). The contours show the interfaces between distinct water masses. The densities are the TW (<25.7), SACW (>25.7 and <26.8), AAIW (>26.8 and <27.53), NADW (>27.53), as proposed by Silveira *et al.* (2000) and Pereira *et al.* (2014). a) GO-SHIP A10 data (October 2011). b) ORAS5 data (October 2011). c) BIAS between GO-SHIP A10 (October 2011) and ORAS5 (October 2011). d to h) θ BIAS between GCMs and ORAS5 (1979-2017). The same description is applied to the SO data Figures i to p.
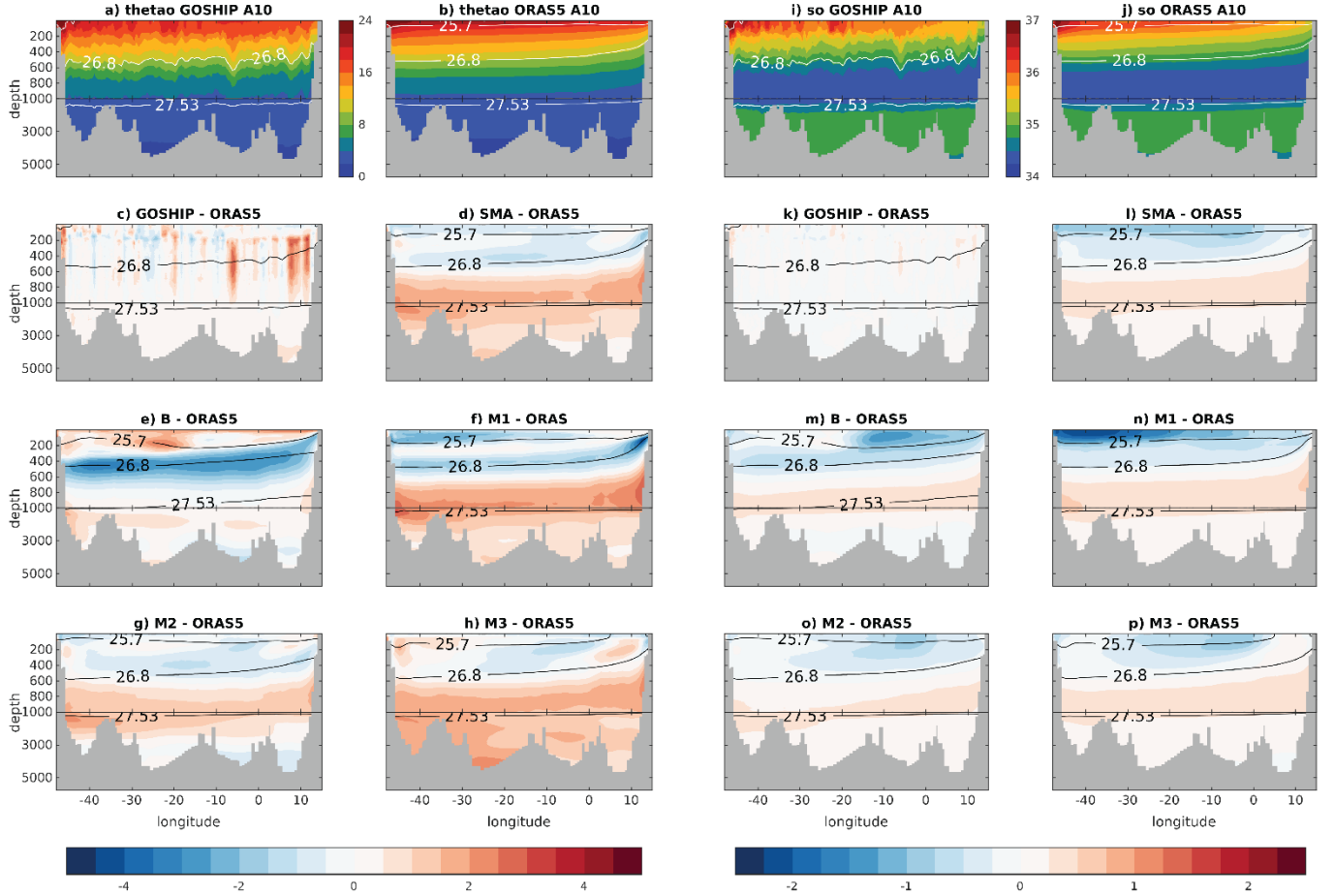
In Figure 5e, the model B can represent all water masses; however, their spatial patterns differ from the ORAS5 data especially in the TW/SACW interface. The B model pattern presented a greater thickness of TW between 0 and 15°W, however, we would expect the highest concentration of this water body region closer to the Brazilian coast due to the presence of the western boundary current. These currents are narrower, thicker and are responsible for transporting TW from the tropical region to the south by the BC (EMÍLSSON, 1961, STRAMMA; ENGLAND, 1999). Positive BIAS of near-surface θ is found between 20 and 30°W. This pattern is not observed in the salinity errors, therefore there is no density compensation. Near to the surface, between 0° and 15°W, negative BIAS occurs in the SO, responsible for overestimating

TW thickness and probably due also to the displacement between water masses since it favors the local density decrease (HELBER; RICHMAN; BARRON, 2010). The poor representation of the SACW can be seen as the main error of the B model, especially due to inaccuracy in θ. Errors at intermediate depths are commonly reflected on the water masses formation (FLATO *et al.*, 2013).

Figure 6 shows the BIAS patterns for salinity and temperature. A similarity between θ and SO patterns are associated with SACW and its formation (Figure 5). This water mass has its main origin associated with the BMCZ. The mixture of Malvinas Current cold waters with runoff Plata river waters promote a sinking and subsequent dispersion in the formed water mass (EMÍLSSON, 1961; SILVEIRA *et al.*, 2000; STRAMMA; ENGLAND, 1999). We identified negative biases peaks between 30°S and 40°S approximately, and a substantial difference in both properties, but little changes in the water mass density. Unlike profile A10, where the effect is not clear; the A16S profile shows a density compensation pattern (TIPPINS; TOMCZAK, 2003). In this case, we notice that the BIAS in SO is more pronounced at surface layers than θ (Figures 6l to 6p), which apparently affects water mass formation.

In both physical properties of the profiles A10 and A16S, B and M2 models provided the representation for waters below 700m depth showing good representations for the AAIW and NADW. In both water masses, the formation has partial influence of the ocean ice (GRIFFIES *et al.*, 2009; STRAMMA; ENGLAND, 1999). The fact that AAIW and NADW have satisfactory simulations in the B model serve as a clue for the good representation of the ice-ocean in the model.

Figure 6. The BIAS between the simulated and reference (ORAS5) θ (Cº) (a-h) and so (l-p) monthly climatology in the South Atlantic Ocean at meridional transect (GO-SHIP A16S). The contours show the interfaces between distinct water masses. The densities are the TW (<25.7), SACW (>25.7 and <26.8), AAIW (>26.8 and <27.53), NADW (>27.53), as proposed by Silveira *et al.* (2000) and Pereira *et al.* (2014). a) GO-SHIP A16S data (October 2011). b) ORAS5 data (October 2011). c) BIAS between GO-SHIP A16S (October 2011) and ORAS5 (October 2011). d to h) θ BIAS between GCMs and ORAS5 (1979-2017). The same description is applied to the SO data in Figures i to p.
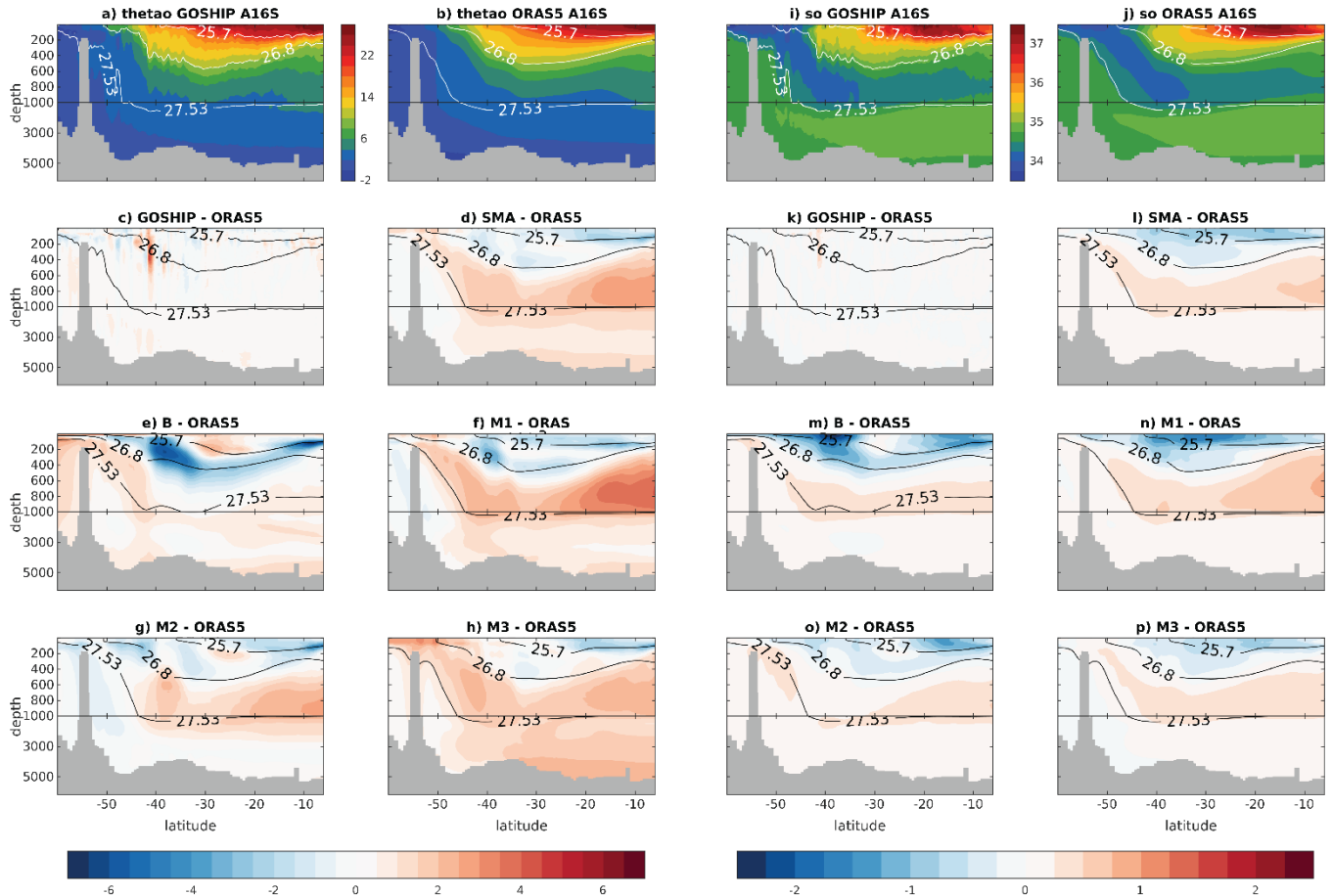

The capacity of GCMs to represent water masses near de Brazilian continental shelf are illustrated in Figure 7, which shows the T-S diagrams for point P (35ºW/21.5ºS) (see Figure 1), a MOVAR station in intermediary zone between Cabo Frio/RJ and the Trindade Island. In Figure 7, the 65 pairs of thermohaline data were obtained by MOVAR expeditions between 2004 and 2017. We discarded the expeditions of June 2011 and January 2014 because of data inconsistency.

Figure 7. T-S diagram for P point, located at the intermediary zone of MOVAR transects (2004-2017). Diagram (a) shows the ORAS5 (black color lines) and MOVAR (gray color lines) comparison. The other diagrams show the CMIP5 (color lines) and MOVAR comparison. The water masses were sectored according to Silveira *et al.* (2000) and Pereira *et al.* (2014).
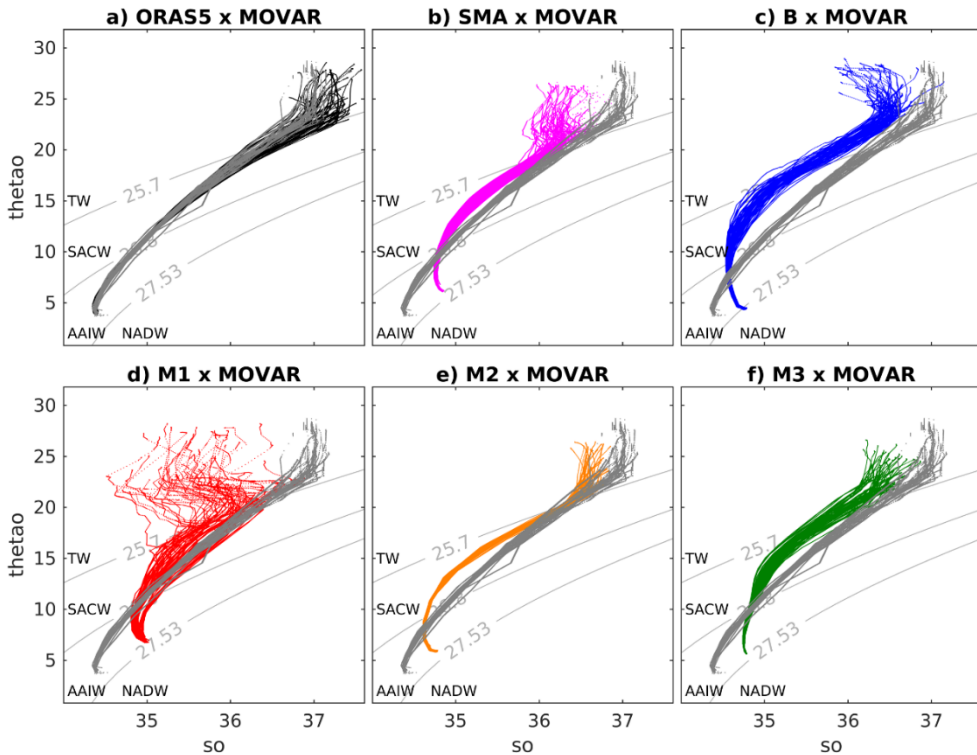
Unlike previous analyses, MOVAR data will be used as reference instead of ORAS5 because the observational program has a concise time series with an excellent quality data control. Data from all seasons are displayed in the same T-S diagram (Figure 7). The comparison between MOVAR and ORAS5 reanalysis (Figure 7a) reinforces the ORAS5 performance viewed in the Figures 2, 5 and 6, where very low BIAS (approximately 0°C and 0 salinity) were found in almost all studied area. In the T-S diagram, the temperature and salinity of the ORAS data show errors only in TW in comparison to MOVAR data. The comparisons between thermohaline data from the MOVAR program and the GCMs are shown in Figure 7b to 7f.

All GCMs models were not able to capture the real values of salinity at the deepest layers since their salinity values were higher than the observed ones. The models B, M2, M3, and SMA have shown similar behaviors in T-S diagrams, while the M1 model, presented the largest discrepancy, especially at surface layers, although the model reproduces better the SACW. All GCMs models simulate the TW and SACW with an increase in temperature and decrease in salinity, generating a slight

displacement of the T-S curve. All the GCMs could not simulate the AAIW with the same salinity and temperature observed values, since the MOVAR data present a more elongated curve, reaching both lower temperatures and salinities. In particular, the B model demonstrated the deep temperature more similar to de reference data.

3.3 SKILL MEASURES

The NRE (Figure 8) will be extensively used here to evaluate the skill of the GCMs. The method was originally described by Gleckler, Taylor and Doutriaux (2008) to compare the physical properties error in model simulations. In the study, we used the NRE method with adaptations made by Pincus *et al.* (2008), which compare the statistical parameters error. The diagram shows how much a model differs from the median of all model errors (TME). If the model has an NRE value of 0.1 (-0.1), then the model error is 10% larger (smaller) than the TME. These model performances are assessed by comparing their thermohaline properties with the reference data (ORAS5).

Many authors discussed the average model performances (ANNAN; HARGREAVES, 2011; GLECKLER; TAYLOR; DOUTRIAUX, 2008; PINCUS *et al.*, 2008; RANDALL *et al.*, 2007; SILLMANN *et al.*, 2013). According to Tebalbi and Knutti (2007), the consistency of the mean ensembles tends to increase as the number of samples or models also grows. If we consider a greater number of the GCMs, errors will probably be suppressed. Therefore, we would expect that either the AMA or the SMA has minor RNEs. This pattern can be seen in SST, θ and SO. By comparing the SMA and AMA data sets, we observed that the first presented a better performance than the second in three (SST, θ and SSS) out of the four evaluated physical properties.

The SO is the only of the evaluated physical properties that presented a satisfactory performance in the B model when compared to the other GCMs. Although some statistical variables such as R, CRMSE or RStdD have shown good NREs values for the models M2 and M3, the RMSE and BIAS have shown that in these models the errors are higher than the TMEs. The NREs for the B model remained close to the TMEs, without any pronounced positive error. However, the B model did not present good performance for SST, θ and SSS. In the case of SST, four metrics presented

NRE close to +100%, demonstrating high errors, and R was the only metric performance with good behavior. The B model performance in representing θ resembled the M1 model, however, we observe that some metrics with positives NREs in the M1 model have even higher values in the B model. All models presented errors for SSS close to the TME but the B model results present the largest errors, mainly in BIAS and RMSE.

Figure 8. Normalized relative error (NRE) portrait diagram of monthly cycles (1979-2017) of the properties SST, SSS, θ, and SO in the South Atlantic Ocean. The columns and rows are represented by GCMs and NRE, respectively, according to the physical parameter. The color gradients represent the NRE magnitudes, where colder (warmer) color represent models with errors below (above) TME. If the color is white, then GCMs errors are similar to TME.
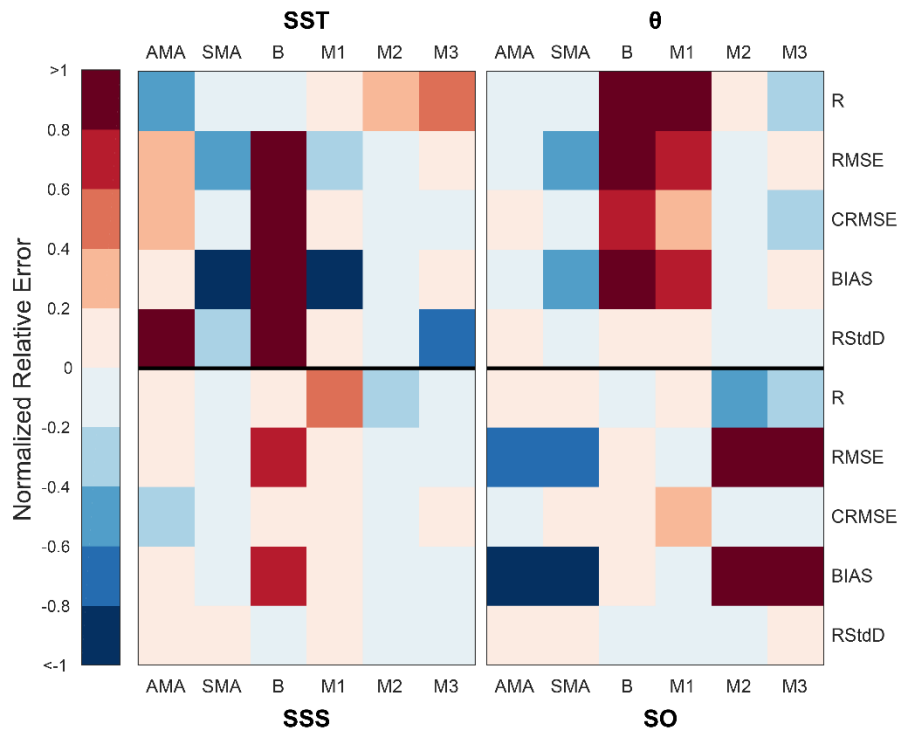
The NREs patterns revealed that the B model errors were usually associated with the amplitudes of the time series variations (residuals between reference data and simulated data), as well as errors seen from their mean. In most of the analyzed properties, except for θ, we observed a good behavior in the variation patterns, associated with the NREs of R, evidencing that the temporal series variations were closed to the models.

It is important to note the changes that occurred between statistical variables. In some situations, it is possible to observe the presence of positive and negative NREs for a determined model corresponding to a single physical property (e.g., M3 model

presented positives or negatives metrics in the SO). This shows how dynamic and complex is the evaluation process of a model. It is also worth noting that the NRE analysis compares the models to the TME, which is generated by the error's central tendency of the models themselves. Thus, performances above or below the median are unavoidable, but this does not mean that models with positive magnitudes should be considered unsatisfactory models.

The Taylor diagram (Figure 9) gives a quantitative representation of the main statistical results of the evaluation process. We normalized the standard deviations of the reference data of the all physical proprieties for the value 2, allowing us to represent several variables in the same diagram, since the point that represent the reference data has the same position for all physical properties. In the Taylor diagram, the origin of radial distances represent the patterns of standard derivations. R is presented in the azimuthal angle, and the observed radial distances are proportional to CRMSE (TAYLOR, 2001).

Figure 9. Taylor diagram showing the performance of the global climate models (GCMs) to estimate the temperature (°C) (SST and θ) and salinity (SSS and SO) monthly means during the period 1979-2017 in the South Atlantic Ocean. The diagram corresponds to the comparisons between ORAS5 and GCMs. Each symbol represents a physical parameter. The reference data (ORAS5) appear plotted along the abscissa axis.
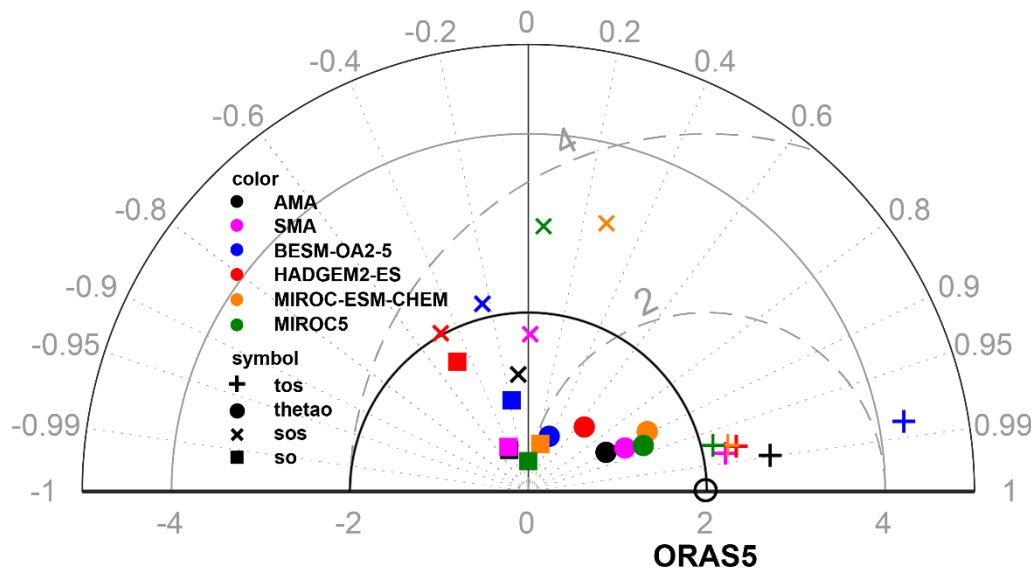
The proximity of SSS and SO parameters in the Taylor diagram is clear, with small differences in their CRMSE values. Both the ensembles to all GCMs shows the worse representation when compared to the temperature data, which statistically

corroborates to the great complexity in simulating this parameter. The SO (SSS) parameter is better represented in the B model than in the M1 (M1 and M3) model. In general, the correlation coefficients of all GCMs were low here and negative in some cases. We observed the reduced SO StdD values in the models, representing the smaller amplitudes compared to the reference data.

The Taylor diagram shows some differences to the calculated NRE shown in Figure 8. We noticed better patterns in the AMA and SMA ensembles only for the SSS and SST properties respectively. In the Taylor diagram, the interference generated by the weighting of some models is clear. For instance, the positions of the B and M1 models for simulating θ and SO are distant to the ORAS5 data, which cause impacts on the behaviors of the mean ensembles (AMA and SMA). This fact can be seen more clearly in the SST property in which we observe that the B model misrepresents the AMA output.

3.4   FUTURE SCENARIOS

Figure 10 shows the annual differences between 2018 and 2098 in SST (Figure 10 [a to d]) and SSS (Figure 10 [e to h]), for the B model and SMA using RCP 4.5 and RCP 8.5, therefore simulations in the spatial patterns of physical properties in the 80 years. It is important to emphasize that this evaluation has shown the differences in property values in the 80-year period, which explains why patterns seen in Figure 2 are not observed here.

We can notice small differences between the B model and SMA, especially in the SST patterns. In both RCPs, the B model provided scenarios with major warming in middle latitude regions (40° S to 60° S); which include the STZ, SAZ, and Polar zone. In the SMA ensemble, the opposite happens with warming in the Tropical zone (TZ). No difference in warming fields was noticed between both RCPs forcing using B and SMA models. Both models exhibit a maximum temperature of about 3 and 6°C for RCP 4.5 and RCP 8.5, respectively, at the end of the simulated period. We noticed many similarities in the SSS increases in both RCPs with a difference in the Gulf of Guinea region, where the SSS abruptly decreased in the SMA ensemble.

Figure 10. Changes between the years of 2098 and 2018 for SST (°C) (a-d) and SSS (e-h). a and e) The differences for the RCP 4.5 scenario using the B model. b and f) The differences for the RCP 8.5 scenario using the B model. c and g) The differences for the RCP 4.5 scenario using SMA model. d and h) The differences for the RCP 8.5 scenario using SMA model.
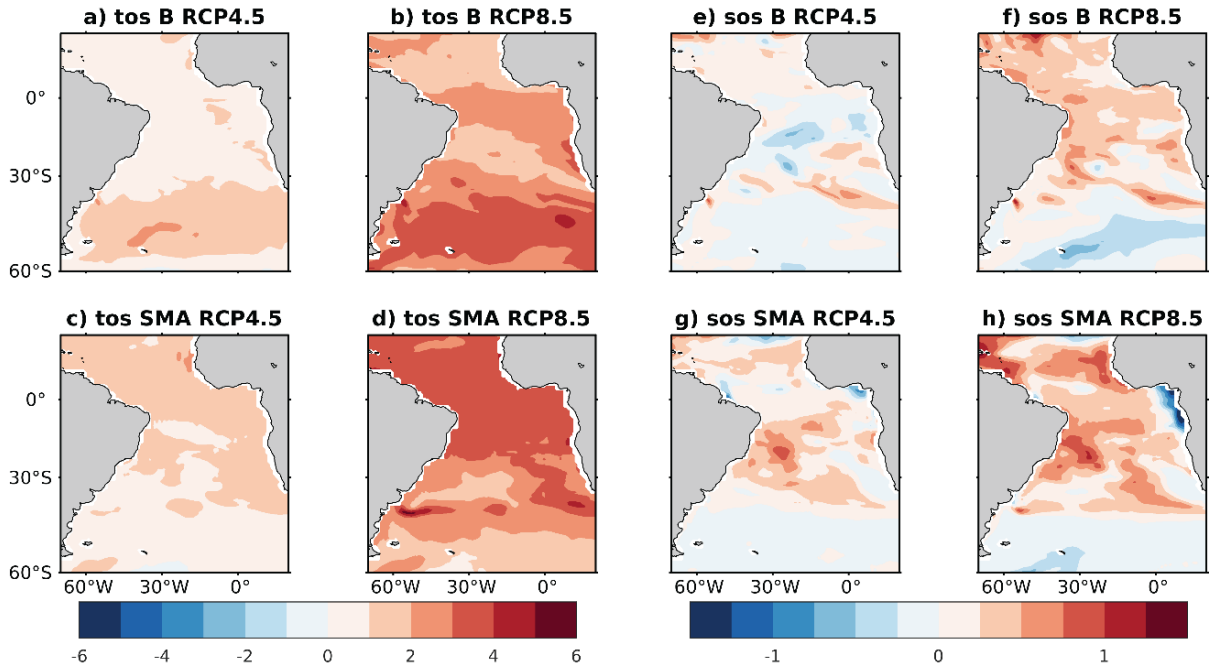
In the climate warming scenario, the water cycle is enhanced and is expressed in the surface water fluxes intensification (evaporation and precipitation), which reflect effects in patterns in salinity, also called "rich get richer" mechanism (CHOU *et al.*, 2006; CHOU *et al.*, 2009; DURACK; WIJFFELS; MATEAR, 2012; TERRAY *et al.*, 2012). The described patterns in SSS fields showed in Figure 10 with salinity increase (decrease) in subtropical (temperate latitude, ~40°S to 60°S) was also described by the authors. The results demonstrated the good spatial representativeness caused by the radiative forcing increase in the GCMs.

Figure 11 presents the linear trends of the SST (a and c) and SSS (b and d) properties in SAO, for the RCPs using all GCMs, including the SMA and AMA.

For both variables SST and SSS, the positive trends seen in the historical data (1979-2017) remain in the future, with the exception for SSS (RCP 8.5) in the M2 model, which shows an increase in the moving averages until approximately the year of 2050 then a decrease resulting in a neutral trend over 80-year period.

Figure 11. Mean monthly SST (°C) and SSS from 2018 to 2098 to RCP 4.5 and RCP 8.5. The straight lines show the linear trends obtained for AMA, SMA, B, M1, M2 and M3 along the 80 years.
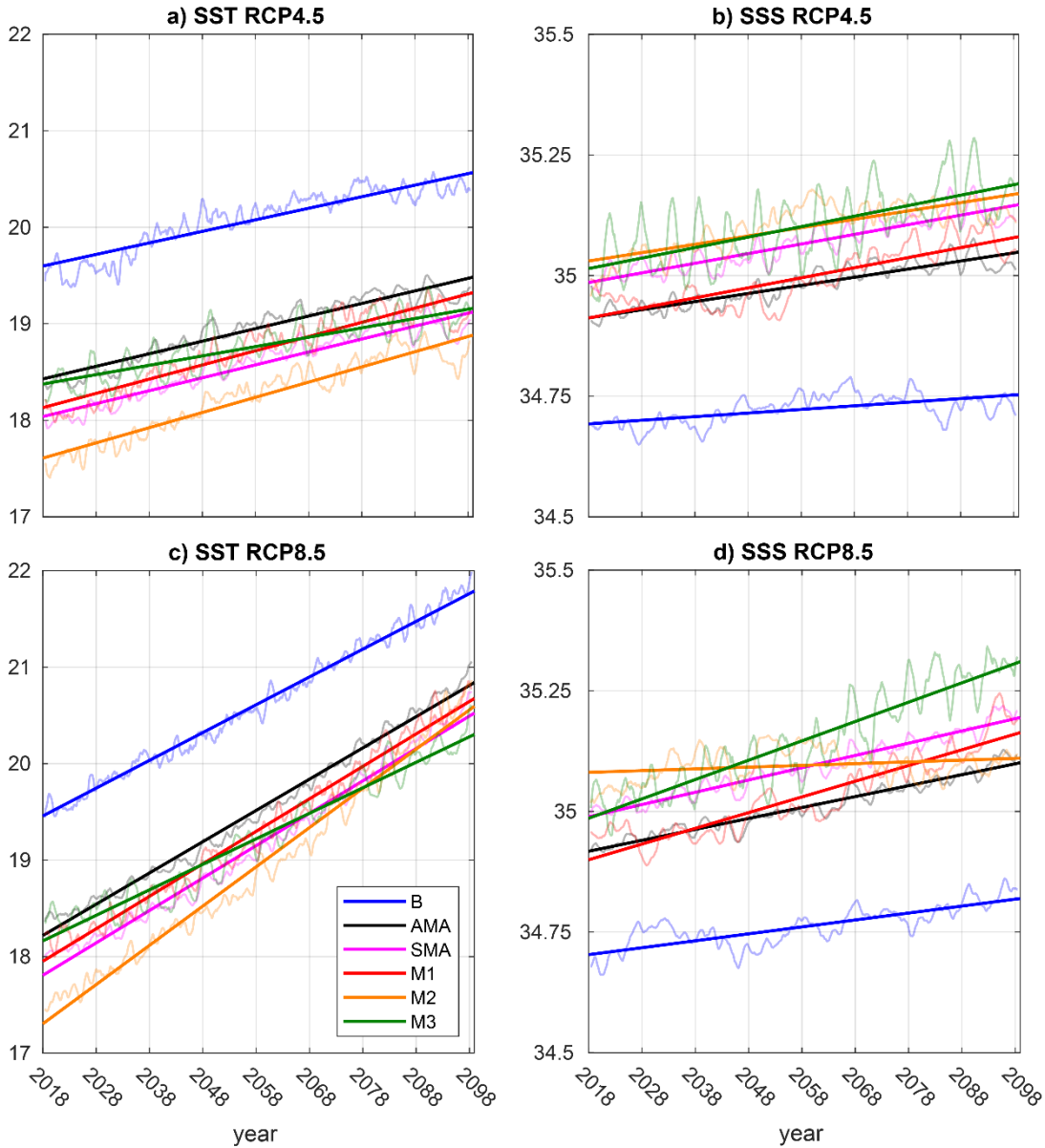
Systematic discrepancies, previously described and especially for the B model, are observed in the two RCPs (Table 4). It is perceptible of the impact of applying two distinct scenarios. The scenarios of the model show the response to the higher emissions and radiation of the RCP 8.5 (Figures 11 [c and d]), representing the intensification of physical properties analyzed. However, due to the smaller slope in the trend lines, it is possible to notice that the model shows more attenuated rates to the others.

Table 4. Rate of variation of both mean annual SST (°C) and SSS and percentage of variation of SST and SSS over the 80 years (2018-2098) in the RCP 4.5 and RCP 8.5 scenarios. The color gradient represents the lowest to highest rate or value. Warmer (colder) shades represent higher (lower) values. The Mann Kendall p-value do not show in this table because all values were equal to 0. PP = Physical Parameter.

PP	RCP	Rate	AMA	SMA	B	M1	M2	M3
SST	4.5	80yrs rate(°C/80years)	1.079	1.101	1.012	1.215	1.289	0.798
		Annual rate(°C/year)	0.013	0.014	0.013	0.015	0.016	0.010
		Mean (°C)	18.957	18.581	20.086	18.728	18.246	18.770
	8.5	80yrs rate(°C/80years)	2.621	2.713	2.348	2.726	3.274	2.138
		Annual rate(°C/year)	0.033	0.034	0.029	0.034	0.041	0.027
		Mean (°C)	19.528	19.163	20.623	19.312	18.946	19.230
SSS	4.5	80yrs rate	0.136	0.160	0.062	0.171	0.138	0.172
		Annual rate	0.0017	0.0020	0.0008	0.0021	0.0017	0.0022
		Mean	34.981	35.067	34.723	34.996	35.101	35.103
	8.5	80yrs rate	0.180	0.202	0.113	0.262	0.026	0.319
		Annual rate	0.0023	0.0025	0.0014	0.0033	0.0003	0.0040
		Mean	35.009	35.092	34.761	35.032	35.096	35.148

The B model simulated a warming of ~1.01°C in 80 years for RCP 4.5 and ~2.35°C for RCP 8.5 scenarios. Similar behavior was also identified for salinity with an increase of 0.062 and 0.113, for the RCPs 4.5 and 8.5 scenarios, respectively. These values indicate the model climatic sensitivity since the trend rates of the B model increase when forced by a more drastic scenario (RCP 8.5). It is worth mentioning that the B model has reasonably small rates compared to all models. As previously mentioned, Nobre *et al.* (2013) highlighted the difficulties of the B model to represent well the variability of atmospheric CO_2. Therefore, the smaller warming rates of the B model might be associated with low sensitivity for CO_2 concentrations changes. This fact can be corroborated with the similarity of the SST rates given by the B and M3 models. The M3 model is not composed of modules of atmospheric chemistry, land carbon and biogeochemical ocean (FLATO *et al.*, 2013), therefore, some processes with CO_2 are not pondered for this model and the assumptions of Nobre *et al.* (2013) are even more plausible.

The SSS can be affected by CO_2 deficit, generating differences in the E-P or sea ice volumes, by the radiative forcing errors. However, the SSS patterns between the B and M3 models diverge. It is hard to say which generates this divergence, because of salinity pattern behavior. Rivers runoff and melting ice may not exert a strong influence since their impacts are spatially restricted (PETERSON *et al.*, 2006;

SCHMITT, 2008). To understand the disparity given by B and M3 models it is necessary to evaluate the components of precipitation and evaporation to recognize the patterns of each model against the changes CO_2 or the radiation forcing of the RCPs.

In general, the B model presented low rates of SSS in both RCPs. The SSS rate simulated by the M2 model in the RCPs 8.5 scenario is also interesting since the salinity rate remains close to a null variation during the 80 years and is the minor rate between all models. Thus, the B model is presented as the nearest variation of all models' average rate, representing a substantial value for the behavior of SSS.

4 CONCLUSIONS

The main goal of this research was to evaluate the performance of BESM and three other GCMs in the South Atlantic Ocean. The models were forced by different radiative forcing and their errors were statistically accessed by comparing with historical referenced data. The spatial patterns of the thermohaline properties were analyzed and their temporal trends were calculated.

The spatial patterns of errors of the B model were similar to the other models, especially in the temperature field, in regions such as the BMCZ, BUS and higher latitudes (ACC, STZ, and SAZ), which reflects the satisfactory behavior of BESM. Nevertheless, a systematic error in temperature was found, mainly during the summertime and this error had a significant impact in mean latitudes regions (30 to 60°S). Assessments such as the trend analyze, the relative normalized errors and the Taylor diagram statistics corroborate to this systematic error. Despite this error, the BESM model has a better historical SST trend rate among all models. A major diversity in the spatial patterns of salinity between GCMs was found already expected because of the difficulty in representing this property. This complexity is reflected in the Taylor diagram. The models had difficulty in representing the rivers runoff both in the eastern and western SAO borders. Specifically, for the B model, more intense negative BIAS was observed in the Subtropical front and higher latitudes, possibly related to evaporation-precipitation balance and existing ocean-ice but with smaller impact. This pattern persists throughout the year leading to a lower mean salinity. In summary, the BESM model shows a good spatial representation along the Brazilian coast and

tropical zone, with SSS little errors in the regions. Due the spatial resolution, we not observed waters incursion over continental shelf in none assessed GCM.

In the subsurface, the B model represented the four main water masses that compose the SASG but with a spatial error of the TW. The deepwater representation was a major highlight in this assessment with AAIW and NADW patterns being very well simulated, and therefore, it is indicative of the well ocean-ice representation of the model. Difficulties in the SACW representation were observed which are associated with the water mass formation where the same error patterns were observed for SSS and SST leading to the density compensation effect. All models showed similar errors about the distribution of water masses along the Brazilian coast when compared with the MOVAR dataset. The B model presented a slight displacement in the T-S curve resulting in an increment in TW. This model represented well the temperature specifically associated with the AAIW. Analysis of Taylor´s diagram, have shown that the B model departs from the reference data, but the normalized relative error analysis showed an error close to the TME, being considered a relevant representation.

In the future scenarios' analysis, we identified the same magnitudes and fields of the SST and SSS increases in both the B and SMA models. However, the B model presented higher mean temperature and lower salinity with trend rates close the smallest among GCMs. The causes of the attenuated impact on the trend rates is probably due to a lower response to the B model to the variations of the atmospheric CO_2 concentration.

The complexity of the global climate models demand continuous evaluations for their improvement. The BESM model were able to reproduce reasonably well the salinity and temperature fields in the Tropical South Atlantic and Brazilian coastal regions, even in intermediate and deep waters. The number of physical properties in the evaluation process should be increased to better clarify the divergences between models observed in this work.

3 CONCLUSÕES

O principal intuito desta pesquisa foi avaliar o modelo BESM e três outros modelos no oceano Atlântico Sul. A componente termohalina foi avaliada a partir dos padrões espaciais dos erros, métricas estatísticas e as suas tendências temporais foram calculadas.

As simulações da reanálise ORAS5 representaram os programas de monitoramentos do oceano com baixos erros, o que a classificou como dado de referência satisfatório.

A análise espacial do modelo BESM demostrou padrões de erros similares aos demais modelos, especialmente nos campos de temperatura, com destaque para regiões como a BMCZ, a BUS e altas latitudes (ACC, STZ e SAZ). Nesta abordagem, ter o mesmo padrão de erro apresentado pelos demais modelos, reflete em um comportamento satisfatório do modelo BESM; porém, um erro sistemático de temperatura foi observado, com maior relevância durante o verão, com impacto expressivo em regiões de médias latitudes (30 a 60°S), provavelmente justificado por erro no balanço radioativo. As análises de tendências, os erros relativos normalizados e a métricas estatísticas aplicadas ao diagrama de Taylor corroboraram este erro sistemático. Apesar disso, o modelo BESM apresentou a melhor tendência histórica de temperatura superficial dentre os modelos analisados. A salinidade superficial apresentou maior diversidade nos padrões espaciais de erros entre os GCMs, algo esperado pela dificuldade de representação que está propriedade física demonstra. Essa complexidade é refletida no diagrama de Taylor. Na análise de salinidade fica clara a dificuldade dos modelos em representar o escoamento de rios, em ambos as bordas do oceano Atlântico Sul. Especificamente, BIAS negativos do modelo B são observados na Subtropical front e latitudes mais altas, possivelmente relacionados ao balanço de evaporação-precipitação e o gelo marinho, com menor impacto. Este padrão persiste durante o ano todo e força tendências com valores mais baixos para esta propriedade física. No geral, o modelo BESM demostrou uma boa representação ao longo da costa brasileira e zona tropical, com pequenos erros de salinidade nestas regiões. Devido as resoluções espaciais dos GCMs, não foi possível observar ou avaliar incursões de água sobre a plataforma continental em nenhum dos modelos analisados.

Em subsuperfície o modelo BESM representou as quatro principais massas d'agua que compõem o SASG, com erro de disposição espacial da TW. A boa representação de águas profundas como AAIW e NADW foram grandes destaques do modelo, servindo como indicativo de boa representação de gelo marinho nas regiões de formação destas massas de água. Dificuldades na representação da SACW foram observadas, com problemas em sua formação, sendo caracterizado efeito de compensação de densidade devido aos mesmos padrões de erros em ambas as propriedades físicas avaliadas. A comparação de massas de água junto a costa brasileira mostrou proximidade entre os modelos na comparação com o conjunto de dados MOVAR. O modelo BESM apresentou um leve deslocamento na curva, causando o incremento de TW na amostragem. Este teve melhor representação da temperatura associado a AAIW. Pela estatística de Taylor, o modelo BESM foi o mais distante da referência, porém, a análise do erro relativo normalizado demonstrou erro próximo ao TME, sendo considerada uma representação relevante.

Na análise de cenários futuros, o modelo BESM mostrou campos de aumentos de SST e SSS em mesma grandeza e padrões espaciais aproximados ao SMA. Este comportamento foi satisfatório, frente as variações impostas pelos cenários RCP 4.5 e 8.5. Apesar do modelo ainda apresentar média maior de temperatura e menores de salinidade, as taxas evolutivas foram em sua maioria, as menores vistas entre os GCMs. A possível causa desta peculiaridade foi a baixa representação do modelo aos impactos de variação na concentração de CO_2 atmosférico. Deste modo, apenas os acréscimos nas forçantes radioativas foram as causas do impacto atenuado sobre as taxas de evolução.

A complexidade de modelos climáticos globais demanda continuas avaliações para seus incrementos e evoluções. Desta forma, a partir deste estudo, é recomendado a ampliação das propriedades físicas na avaliação do modelo BESM, com o intuito de esclarecer as divergências apresentadas e propiciar melhores embasamentos e resultados.

A partir dos resultados atingidos por este estudo, é plausível o uso do modelo BESM em simulações de campos de temperatura e salinidade em regiões como a costa brasileira e Atlântico Sul Tropical, além do uso do mesmo para simulações da dinâmica de águas profundas, como a AAIW e NADW. O uso do mesmo faz-se útil em estudos de previsões e mensurações dos impactos das mudanças climáticas nestas

regiões, servindo como ferramenta principal ou como entrada de dados (condições de contorno) em modelos regionalizados.

REFERÊNCIAS

ANNAN, J. D.; HARGREAVES, J. C.. Understanding the CMIP3 multimodel ensemble. **Journal of Climate**, v. 24, n. 16, p.4529-4538, 2011. American Meteorological Society. http://dx.doi.org/10.1175/2011jcli3873.1.

BARBERO, L.; WANNINKHOF, R.. **GO-SHIP A16S, 23 December 2013-04 February 2014:** CLIVAR and Carbon Hydrographic Data Office (CCHDO). 2014. Disponível em: <https://cchdo.ucsd.edu/search?q=GO-SHIP>. Acesso em: abr. 2018.

BADER, D. C. *et al.* **Climate models:** An assessment of strengths and limitations. 3: Geological and Atmospheric Sciences Reports, 2008. 123 p..

BARNES, W. L.; PAGANO, T. S.; SALOMONSON, V. S.. Prelaunch characteristics of the moderate resolution imaging spectroradiometer (MODIS) on EOS-AM1. **Ieee Transactions on Geoscience and Remote Sensing**, v. 36, n. 4, p.1088-1100, 1998. Institute of Electrical and Electronics Engineers (IEEE). http://dx.doi.org/10.1109/36.700993.

BERGER, H. *et al.* Dynamical contribution to sea surface salinity variations in the eastern Gulf of Guinea based on numerical modelling. **Climate Dynamics**, v. 43, n. 11, p.3105-3122, 2014. Springer Nature. http://dx.doi.org/10.1007/s00382-014-2195-4.

CASAGRANDE, F. *et al.* Arctic sea ice: Decadal simulations and future scenarios using BESM-OA. **Atmospheric and Climate Sciences**, v. 06, n. 02, p.351-366, 2016. Scientific Research Publishing, Inc,. http://dx.doi.org/10.4236/acs.2016.62029.

CHOU, C. *et al.* Regional tropical precipitation change mechanisms in ECHAM4/OPYC3 under global warming*. **Journal of Climate**, v. 19, n. 17, p.4207-4223, 2006. American Meteorological Society. http://dx.doi.org/10.1175/jcli3858.1.

CHOU, C. *et al.* Evaluating the "rich-get-richer" mechanism in tropical precipitation change under global warming. **Journal of Climate**, v. 22, n. 8, p.1982-2005, 2009. American Meteorological Society. http://dx.doi.org/10.1175/2008jcli2471.1.

CHOU, S. C. *et al.* Evaluation of the Eta simulations nested in three global climate models. **American Journal of Climate Change**, v. 03, n. 05, p.438-454, 2014. Scientific Research Publishing, Inc,. http://dx.doi.org/10.4236/ajcc.2014.35039.

COLLINS, W. J. *et al.* Development and evaluation of an earth-system model – HadGEM2. **Geoscientific Model Development**, v. 4, n. 4, p.1051-1075, 2011. Copernicus GmbH. http://dx.doi.org/10.5194/gmd-4-1051-2011.

DURACK, P. J.; WIJFFELS, S. E.; MATEAR, R. J.. Ocean salinities reveal strong global water cycle Intensification during 1950 to 2000. **Science**, v. 336, n. 6080, p.455-458, 2012. American Association for the Advancement of Science (AAAS). http://dx.doi.org/10.1126/science.1212222.

EMÍLSSON, I.. The shelf and coastal waters off southern Brazil. **Boletim do Instituto Oceanográfico**, v. 11, n. 2, p.101-112, 1961. FapUNIFESP (SciELO). http://dx.doi.org/10.1590/s0373-55241961000100004.

EUROPEAN CENTRE FOR MEDIUM-RANGE WEATHER FORECASTS (ECMWF). **Ocean ReAnalysis System 5 (ORAS5):** Integrated Climate Data Center. 2017. Disponível em:

<http://icdc.cen.uni-hamburg.de/1/projekte/easy-init/easy-init-ocean.html?no_cache=1>.   Acesso em: abr. 2018.

EYRING, *et al.* Overview of the coupled model intercomparison project phase 6 (CMIP6) experimental design and organization. **Geoscientific Model Development**, v. 9, n. 5, p.1937-1958, 2016. Copernicus GmbH. http://dx.doi.org/10.5194/gmd-9-1937-2016.

FARIAS, E. G. G. de *et al.* Variability of air-sea CO2 fluxes and dissolved inorganic carbon distribution in the Atlantic Basin: A coupled model analysis. **International Journal of Geosciences**, v. 04, n. 01, p.249-258, 2013. Scientific Research Publishing, Inc,. http://dx.doi.org/10.4236/ijg.2013.41a022.

FATHRIO, I. *et al.* Evaluation of CMIP5 models on sea surface salinity in the Indian Ocean. **Iop Conference Series:** Earth and Environmental Science, v. 54, p.1-11, 2017. IOP Publishing. http://dx.doi.org/10.1088/1755-1315/54/1/012039.

FLATO, G. *et al.* Evaluation of climate models. In: STOCKER, T. F. *et al.* **Climate change 2013:** The physical science basis. Contribution of working group I to the fifth assessment report of the intergovernmental panel on climate change. Cambridge, United Kingdom e New York: Cambridge University Press, 2013. Cap. 9. p. 741-866. Cambridge University Press. http://dx.doi.org/10.1017/cbo9781107415324.020.

GARZOLI, S. L.; MATANO, R.. The South Atlantic and the Atlantic Meridional Overturning Circulation. **Deep Sea Research Part II**: Topical Studies in Oceanography, v. 58, n. 17-18, p.1837-1847, 2011. Elsevier BV. http://dx.doi.org/10.1016/j.dsr2.2010.10.063.

GIAROLLA, E. *et al.* Equatorial Atlantic Ocean dynamics in a coupled ocean–atmosphere model simulation. **Ocean Dynamics**, v. 65, n. 6, p.831-843, 2015. Springer Nature. http://dx.doi.org/10.1007/s10236-015-0836-8.

GLECKLER, P. J.; TAYLOR, K. E.; DOUTRIAUX, C.. Performance metrics for climate models. **Journal of Geophysical Research**, v. 113, n. 6, p.1-20, 2008. American Geophysical Union (AGU). http://dx.doi.org/10.1029/2007jd008972.

GODDARD SPACE FLIGHT CENTER, OCEAN ECOLOGY LABORATORY, OCEAN BIOLOGY PROCESSING GROUP (NASA). **SAC-D/Aquarius monthly Sea Surface Salinity Data:** NASA's OceanColor Web. 2014a. Disponível em: <https://oceancolor.gsfc.nasa.gov/l3/>. Acesso em: abr. 2018.

GODDARD SPACE FLIGHT CENTER, OCEAN ECOLOGY LABORATORY, OCEAN BIOLOGY PROCESSING GROUP (NASA). **Moderate-resolution Imaging Spectroradiometer (MODIS) Aqua monthly Sea Surface Temperature Data**: NASA's OceanColor Web. 2014b. Disponível em: <https://oceancolor.gsfc.nasa.gov/l3/>. Acesso em: abr. 2018.

GODDARD SPACE FLIGHT CENTER, OCEAN ECOLOGY LABORATORY, OCEAN BIOLOGY PROCESSING GROUP (NASA). **Moderate-resolution Imaging Spectroradiometer (MODIS) Terra monthly Sea Surface Temperature Data**: NASA's OceanColor Web. 2014c. Disponível em: <https://oceancolor.gsfc.nasa.gov/l3/>. Acesso em: abr. 2018.

GOES, M. *et al.* Long-term monitoring of the Brazil current transport at 22°S from XBT and altimetry data: seasonal, interannual, and extreme variability. **Journal of Geophysical Research**: Oceans, p.3645-3667, 2019. American Geophysical Union (AGU). http://dx.doi.org/10.1029/2018jc014809.

GORDON, A. L.. Interocean exchange of thermocline water. **Journal of Geophysical Research**, v. 91, n. 4, p.5037-5046, 1986. American Geophysical Union (AGU). http://dx.doi.org/10.1029/jc091ic04p05037.

GRIFFIES, S. M. *et al.* Coordinated ocean-ice reference experiments (COREs). **Ocean Modelling**, v. 26, n. 1-2, p.1-46, 2009. Elsevier BV. http://dx.doi.org/10.1016/j.ocemod.2008.08.007.

HELBER, R. W.; RICHMAN, J. G.; BARRON, C. N.. The influence of temperature and salinity variability on the upper ocean density and mixed layer. **Ocean Science Discussions**, v. 7, n. 4, p.1469-1495, 2010. Copernicus GmbH. http://dx.doi.org/10.5194/osd-7-1469-2010.

HOOD, M. *et al.* Ship-based repeat hydrography: A strategy for a sustained global program. **Proceedings of Oceanobs'09**: Sustained ocean observations and information for society, 2010. European Space Agency. http://dx.doi.org/10.5270/oceanobs09.cwp.44.

HUTCHINGS, L. *et al.* The Benguela current: An ecosystem of four components. **Progress in Oceanography**, v. 83, n. 1-4, p.15-32, 2009. Elsevier BV. http://dx.doi.org/10.1016/j.pocean.2009.07.046.

LANDERER, F. W.; GLECKLER, P. J.; LEE, T.. Evaluation of CMIP5 dynamic sea surface height multi-model simulations against satellite observations. **Climate Dynamics**, v. 43, n. 5-6, p.1271-1283, 2013. Springer Science and Business Media LLC. http://dx.doi.org/10.1007/s00382-013-1939-x.

LAGERLOEF, G. *et al.* The Aquarius/SAC-D mission: Designed to meet the salinity remote-sensing challenge. **Oceanography**, v. 21, n. 1, p.68-81, 2008. The Oceanography Society. http://dx.doi.org/10.5670/oceanog.2008.68

MACDONALD, A.; BARINGER, M. O.. **GO-SHIP A10, 26 September 2011-31 October 2011:** CLIVAR and carbon hydrographic data office (CCHDO). 2011. Disponível em: <https://cchdo.ucsd.edu/search?q=GO-SHIP>. Acesso em: abr. 2018.

MARCELLO, F.; WAINER, I.; RODRIGUES, R. R.. South Atlantic Subtropical Gyre late twentieth century changes. **Journal of Geophysical Research**: Oceans, v. 123, n. 8, p.5194-5209, ago. 2018. American Geophysical Union (AGU). http://dx.doi.org/10.1029/2018jc013815.

MARTIN, G. M. *et al.* The HadGEM2 family of Met Office Unified Model climate configurations. **Geoscientific Model Development**, v. 4, n. 3, p.723-757, 2011. Copernicus GmbH. http://dx.doi.org/10.5194/gmd-4-723-2011.

MEEHL, G. A. *et al.* Global climate projections. In: SOLOMON, S. *et al.* **Climate change 2007**: The physical science basis. Contribution of working group I to the fourth assessment report of the intergovernmental panel on climate change. Cambridge, United Kingdom e New York: Cambridge University Press, 2007. Cap. 8. p. 747-845. Cambridge University Press.

MÖLLER, O. O. *et al.* The effects of river discharge and seasonal winds on the shelf off southeastern South America. **Continental Shelf Research**, v. 28, n. 13, p.1607-1624, 2008. Elsevier BV. http://dx.doi.org/10.1016/j.csr.2008.03.012.

MOSS, R. H. *et al.* The next generation of scenarios for climate change research and assessment. **Nature**, v. 463, n. 7282, p.747-756, 2010. Springer Nature. http://dx.doi.org/10.1038/nature08823.

NACIONAL OCEANIC AND ATMOSPHERIC ADMINISTRATION (NOAA), ATLANTIC OCEANOGRAPHIC AND METEOROLOGICAL LABORATORY (AOML). **AX97 XBT:** Global

Ocean Observing System Brasil (GOOS-Brasil). 2004. Disponível em: <http://www.goosbrasil.org/movar/dados/ or https://www.aoml.noaa.gov/phod/hdenxbt/ax_home.php?ax=97>. Acesso em: abr. 2018.

NOBRE, P. *et al.* Climate simulation and change in the Brazilian climate model. **Journal of Climate**, v. 26, n. 17, p.6716-6732, 2013. American Meteorological Society. http://dx.doi.org/10.1175/jcli-d-12-00580.1.

PEREZ, J. *et al.* Evaluating the performance of CMIP3 and CMIP5 global climate models over the north-east Atlantic region. **Climate Dynamics**, v. 43, n. 9-10, p.2663-2680, 2014. Springer Science and Business Media LLC. http://dx.doi.org/10.1007/s00382-014-2078-8.

PETERSON, R. G.; STRAMMA, L.. Upper-level circulation in the South Atlantic Ocean. **Progress in Oceanography**, v. 26, n. 1, p.1-73, 1991. Elsevier BV. http://dx.doi.org/10.1016/0079-6611(91)90006-8.

PETERSON, B. J. *et al.* Trajectory shifts in the Arctic and Subarctic freshwater cycle. **Science**, v. 313, n. 5790, p.1061-1066, 2006. American Association for the Advancement of Science (AAAS). http://dx.doi.org/10.1126/science.1122593.

PEZZI, L. P.; SOUZA, R. B de; QUADRO, M. F. L.. Uma revisão dos processos de interação oceano-atmosfera em regiões de intenso gradiente termal do Oceano Atlântico Sul baseada em dados observacionais. **Revista Brasileira de Meteorologia**, v. 31, n. 4, p.428-453, 2016. FapUNIFESP (SciELO). http://dx.doi.org/10.1590/0102-778631231420150032.

PINCUS, R. *et al.* Evaluating the present-day simulation of clouds, precipitation, and radiation in climate models. **Journal of Geophysical Research**, v. 113, n. D14, p.1-10, 2008. Wiley-Blackwell. http://dx.doi.org/10.1029/2007jd009334.

PIOLA, A. R. *et al.* The influence of the Plata River discharge on the western South Atlantic shelf. **Geophysical Research Letters**, v. 32, n. 1, p.1-4, 2005. American Geophysical Union (AGU). http://dx.doi.org/10.1029/2004gl021638.

PIOLA, A. R.; MATANO, R. P.. Ocean currents: Atlantic Western boundary—Brazil current/Falkland (Malvinas) current. **Reference Module in Earth Systems and Environmental Sciences**, p.1-6, 2017. Elsevier. http://dx.doi.org/10.1016/b978-0-12-409548-9.10541-x.

RANDALL, D. A. *et al.* Climate models and their evaluation. In: SOLOMON, S. *et al.* **Climate change 2007**: The physical science basis. Contribution of working group I to the fourth assessment report of the intergovernmental panel on climate change. Cambridge, United Kingdom e New York: Cambridge University Press, 2007. Cap. 8. p. 590-662. Cambridge University Press.

ROSSI-WONGTSCHOWSKI, C. L. del B.; MADUREIRA, L. S. P. **O ambiente oceanográfico da plataforma continental e do talude na região sudeste-sul do Brasil.** São Paulo/SP: Edusp, 2006. 466 p.

SALLÉE, J.-b. *et al.* Assessment of Southern Ocean mixed-layer depths in CMIP5 models: historical bias and forcing response. **Journal of Geophysical Research:** Oceans, v. 118, n. 4, p.1845-1862, abr. 2013. American Geophysical Union (AGU). http://dx.doi.org/10.1002/jgrc.20157.

SCHMITT, R. W.. The ocean component of the global water cycle. **Reviews of Geophysics**, v. 33, n. 2, p.1395-1409, 1995. American Geophysical Union (AGU). http://dx.doi.org/10.1029/95rg00184.

SCHMITT, R. Salinity and the global water cycle. **Oceanography**, v. 21, n. 1, p.12-19, 2008. The Oceanography Society. http://dx.doi.org/10.5670/oceanog.2008.63.

SILLMANN, J. *et al.* Climate extremes indices in the CMIP5 multimodel ensemble: Part 1. Model evaluation in the present climate. **Journal of Geophysical Research**: Atmospheres, v. 118, n. 4, p.1716-1733, 2013. American Geophysical Union (AGU). http://dx.doi.org/10.1002/jgrd.50203.

SILVEIRA, I. C. A. da *et al.* A corrente do Brasil ao largo da costa leste brasileira. **Revista Brasileira de Oceanografia**, v. 48, n. 2, p.171-183, 2000. FapUNIFESP (SciELO). http://dx.doi.org/10.1590/s1413-77392000000200008.

STRAMMA, L.; ENGLAND, M.. On the water masses and mean circulation of the South Atlantic Ocean. **Journal of Geophysical Research**: Oceans, v. 104, n. 9, p.20863-20883, 1999. Wiley-Blackwell. http://dx.doi.org/10.1029/1999jc900139.

TALLEY, L. D. *et al.* Atlantic Ocean. **Descriptive Physical Oceanography:** an introduction. California, USA: Academic Press. v. 6, p.245-301, 2011. Academic Press. http://dx.doi.org/10.1016/b978-0-7506-4552-2.10009-5.

TAYLOR, K. E.. Summarizing multiple aspects of model performance in a single diagram. **Journal of Geophysical Research: Atmospheres**, v. 106, n. 7, p.7183-7192, 2001. Wiley-Blackwell. http://dx.doi.org/10.1029/2000jd900719.

TAYLOR, K. E.; STOUFFER, R. J.; MEEHL, G. A.. An overview of CMIP5 and the experiment design. **Bulletin of the American Meteorological Society**, v. 93, n. 4, p.485-498, 2012. American Meteorological Society. http://dx.doi.org/10.1175/bams-d-11-00094.1.

TEBALDI, C.; KNUTTI, R.. The use of the multi-model ensemble in probabilistic climate projections. **Philosophical Transactions of The Royal Society A**: Mathematical, Physical and Engineering Sciences, v. 365, n. 1857, p.2053-2075, 2007. The Royal Society. http://dx.doi.org/10.1098/rsta.2007.2076.

TERRAY, L. *et al.* Near-surface salinity as nature's rain gauge to detect human influence on the tropical water cycle. **Journal of Climate**, v. 25, n. 3, p.958-977, 2012. American Meteorological Society. http://dx.doi.org/10.1175/jcli-d-10-05025.1.

TIPPINS, D.; TOMCZAK, M.. Meridional turner angles and density compensation in the upper ocean. **Ocean Dynamics**, v. 53, n. 4, p.332-342, 2003. Springer Nature. http://dx.doi.org/10.1007/s10236-003-0056-5.

TZORTZI, E. *et al.* Tropical Atlantic salinity variability: New insights from SMOS. **Geophysical Research Letters**, v. 40, n. 10, p.2143-2147, 2013. American Geophysical Union (AGU). http://dx.doi.org/10.1002/grl.50225.

VAN CASPEL, M. R.; MATA, M. M.; CIRANO, M.. Sobre a relação TS na porção central do Atlântico Sudoeste: uma contribuição para o estudo da variabilidade oceânica no entorno da cadeia Vitória-Trindade. **Atlântica**, v. 32, n. 1, p.95-110, 2010. Instituto de Oceanografia - FURG. http://dx.doi.org/10.5088/atl.2010.32.1.95.

WATANABE, M. *et al.* Improved climate simulation by MIROC5: Mean states, variability, and climate sensitivity. **Journal of Climate**, v. 23, n. 23, p.6312-6335, 2010. American Meteorological Society. http://dx.doi.org/10.1175/2010jcli3679.1.

WATANABE, S. *et al.* MIROC-ESM 2010: Model description and basic results of CMIP5-20c3m experiments. **Geoscientific Model Development**, v. 4, n. 4, p.845-872, 2011. Copernicus GmbH. http://dx.doi.org/10.5194/gmd-4-845-2011.

YU, L.. A global relationship between the ocean water cycle and near-surface salinity. **Journal of Geophysical Research**, v. 116, n. 10, p.1-17, 2011. American Geophysical Union (AGU). http://dx.doi.org/10.1029/2010jc006937.

ZHENG, Y. *et al.* Sea surface temperature biases under the stratus cloud deck in the Southeast Pacific Ocean in 19 IPCC AR4 Coupled General Circulation Models. **Journal of Climate**, v. 24, n. 15, p.4139-4164, 2011. American Meteorological Society. http://dx.doi.org/10.1175/2011jcli4172.1.

ZUO, H. *et al.* The ECMWF operational ensemble reanalysis-analysis system for ocean and sea-ice: a description of the system and assessment. **Ocean Science Discussions**, v. 15, n. 3, p.779-808, 2019. Copernicus GmbH. http://dx.doi.org/10.5194/os-2018-154.

APÊNDICE A – KEY POINTS

- Temperature and salinity systematics errors are shown by the BESM model probably due to radiative forcing errors.
- The BESM model demonstrates a good ability to reproduce deeper water masses (Antarctic Intermediate Water and North Atlantic Deep Water).
- The Spatial patterns and trend rates of the BESM model are similar to the other models for the dataset scenarios.

APÊNDICE B – PLAIN LANGUAGE SUMMARY

Numeric models are tools that seek to reproduce any physical process from mathematical equations. Thus, we can use them to reproduce the earth current and future climate, and the climate change. The work evaluates the BESM numeric model efficiency in the current and future climate in the South Atlantic Ocean, using sea temperature and salinity for the analyses. We joined the BESM model to three well-known models similar to it. The four models were compared to a more precise numeric model, to the satellite measures, and the observed measurements from oceanographic instruments. The results show that the BESM model estimated the surface ocean currents well; however, it represented the South Atlantic Ocean hotter and with minor salinity than expected. Below 700m, the model reproduced temperature and salinity better than the other models; however, between the surface and above 700m, we observed errors in these variables. We also measured annual temperature and salinity variations for the present (1979-2017) and the future (2018-2098). The BESM model stood out with the temperature closest to the real from the present; however, it had the errors from salinity. The future annual variations have shown good results, with closer values to the other evaluated models.

APÊNDICE C – ACKNOWLEDGMENTS